Downregulation of ribosome biogenesis during early forebrain development

Kevin F. Chau[1,2], Morgan L. Shannon[1], Ryann M. Fame[1], Erin Fonseca[1], Hillary Mullan[1], Matthew B. Johnson[3], Anoop K. Sendamarai[1], Mark W. Springel[1], Benoit Laurent[4], Maria K. Lehtinen[1,2,*]

[1]Department of Pathology, Boston Children's Hospital, Boston, Massachusetts, 02115, USA

[2]Program in Biological and Biomedical Sciences, Harvard Medical School, Boston, Massachusetts, 02115, USA

[3]Division of Genetics, Boston Children's Hospital, Boston, Massachusetts, 02115, USA

[4]Division of Newborn Medicine and Epigenetics Program, Department of Medicine, Boston Children's Hospital, and Department of Cell Biology, Harvard Medical School, Boston, Massachusetts, 02115, USA

*Correspondence should be addressed to: maria.lehtinen@childrens.harvard.edu

ABSTRACT

Forebrain precursor cells are dynamic during early brain development, yet the underlying molecular changes remain elusive. We observed major differences in transcriptional signatures of precursor cells from mouse forebrain at embryonic days E8.5 vs. E10.5 (before vs. after neural tube closure). Genes encoding protein biosynthetic machinery were strongly downregulated at E10.5. This was matched by decreases in ribosome biogenesis and protein synthesis, together with age-related changes in proteomic content of the adjacent fluids. Notably, c-MYC expression and mTOR pathway signaling were also decreased at E10.5, providing a potential driver for the effects on ribosome biogenesis and protein synthesis. Interference with c-MYC at E8.5 prematurely decreased ribosome biogenesis, while persistent c-MYC expression in cortical progenitors increased transcription of protein biosynthetic machinery and enhanced ribosome biogenesis, as well as enhanced progenitor proliferation leading to subsequent macrocephaly. These findings indicate large, coordinated changes in molecular machinery of forebrain precursors during early brain development.

INTRODUCTION

Neural tube closure (neurulation) is a fundamental milestone of early brain development, yet relatively little is known about the cellular and molecular transitions occurring in neural precursor cells before and after this process due to experimental challenges inherent to investigating this nascent organ (Greene and Copp, 2014; Massarwa and Niswander, 2013; Wallingford et al., 2013; Wilde et al., 2014). Prior to neural tube closure, the neural plate is home to multipotent neural stem cells, including forebrain neurectodermal precursor cells. After neural tube closure, these neurectodermal precursors become progressively lineage restricted as neuroepithelial cells, and then radial glial cells, ultimately giving rise to all neurons and glia in the adult forebrain (Bjornsson et al., 2015). As these progenitors proliferate, their spatial patterning serves as a blueprint for the maturing brain (Rallu et al., 2002; Sur and Rubenstein, 2005). While genes involved in driving the more mature stages of forebrain development are becoming better understood, remarkably little is known about the key genes orchestrating the function of earlier neurectodermal precursors.

While transcriptional regulation is essential for the specification and maturation of the early forebrain, less is known about the dynamics of protein biosynthesis at this early stage. Recent studies have begun to explore how regulated protein synthesis is critical for the successful construction and function of healthy cells and organs (Fujii et al., 2017; Kondrashov et al., 2011; Pilaz et al., 2016; Rasin and Silver, 2016; Shi and Barna, 2015). In turn, the regulation of protein biosynthetic machinery has emerged as a tunable program that can instruct cellular transitions between stem cell dormancy, proliferation, and differentiation (DeBoer et al., 2013; Fujii et al., 2017; Khajuria et al., 2018; Kraushar et al., 2016; Sanchez et al., 2016; Scognamiglio et al., 2016). Mutations in genes encoding ribosomal proteins are associated with

neural tube closure defects (NTD; Greene and Copp, 2014; Wilde et al., 2014), suggesting that regulation of protein biosynthesis is critical during the earliest stages of forebrain development as well. Proteomic analyses have also revealed that ribosomal and translational proteins are elevated in amniotic fluid (AF) prior to neurulation, and are substantially decreased in nascent cerebrospinal fluid (CSF) following neurulation (Chau et al., 2015). However, the mechanisms leading to these changes in the AF and CSF proteomes remain incompletely understood, as this developmental stage precedes choroid plexus development and its secretion of factors into the CSF (Hunter and Dymecki, 2007; Lehtinen et al., 2011; Lun et al., 2015).

Here, we used RNA sequencing to reveal the transcriptomic signature of presumptive forebrain precursor cells before and after neurulation. High expression of the protein biosynthetic machinery together with elevated protein synthesis emerged as a signature of early neural precursors. These transcriptional and cell biological changes closely mirrored proteomic changes in the adjacent AF and CSF. Many genes that were downregulated after neurulation are known, direct targets of the transcription factor c-MYC (hereafter MYC) in other cell types (Ben-Porath et al., 2008; Zeller et al., 2003). Accordingly, MYC modulated ribosome biogenesis in forebrain precursors. Its forced, persistent expression in neural progenitors by mouse genetics approaches increased transcription of protein biosynthetic machinery and was accompanied by increased proliferation of radial glial progenitors leading to macrocephaly by birth. Taken together, our data identify regulation of protein biosynthetic machinery as an important signature of early forebrain development.

RESULTS

Transcriptome signature of early forebrain neuroepithelium

To define the identity and biology of developing forebrain neuroepithelial cells, we microdissected the neuroepithelium away from the adjacent mesenchyme and surface ectoderm in E8.5 and E10.5 embryos (**Figure 1A**, Chau et al., 2015), and performed next-generation RNA sequencing (RNAseq) analysis (**Figure 1**). Gene expression analysis identified 3,898 genes ($q<0.05$) with significantly different expression patterns between the two ages, with 2,375 genes enriched in E8.5 neuroepithelium, and 1,523 genes enriched in E10.5 neuroepithelium (**Figure 1B, Figure 1-figure supplement 1A**).

Among the differentially expressed genes, many were secreted factors and receptors involved in signaling pathways with cardinal roles in brain development including WNT and BMP/TGFβ (**Figure 1C, D, Supplementary File 1**; Monuki, 2007; Sur and Rubenstein, 2005; Wilde et al., 2014). Some secreted factors (e.g. BMP1 and SHH) were enriched in both E10.5 progenitors and CSF, suggesting their secretion into the adjacent fluid (**Supplementary File 1**; Chau et al., 2015), while factors known to be involved in organismal development and neural tube closure including *Wnt5a* and *Pax3* were enriched in E8.5 (**Supplementary File 1**). Differential gene expression was further validated by quantitative RT-PCR (qRT-PCR) on 81 genes including transcription factors, cell surface receptors, and secreted factors, many of which showed an overall positive correlation (**Figure 1-figure supplement 1B**). Expression of *Glast* and *Blbp* were enriched in E10.5 progenitors, indicating the transition from neuroepithelial cells to radial glial cells (**Figure 1-figure supplement 1C**).

We next determined the biological functions of the most differentially expressed genes at each age. Consistent with the progressive lineage restriction of progenitors, initiation of

neurogenesis, and patterning of the brain, the most enriched gene category at E10.5 related to neuronal differentiation (e.g. *Ngn1, Blbp, Glast, Tbr2, Bmp4*; **Figure 1F, Supplementary File 1**). However, unexpectedly, the three most enriched gene categories in E8.5 neuroepithelium were related to protein biosynthetic machinery (**Figure 1E, Supplementary File 1**) and included genes encoding ribosomal proteins (e.g. *Rpl24*), genes involved in ribosome biogenesis (e.g. *Fbl, Dkc1*), and translation factors (e.g. *Eif4e*). Gene set enrichment analysis (GSEA; Subramanian et al., 2005) further confirmed that genes involved in ribosome biogenesis and protein synthesis were significantly enriched in E8.5 progenitors (**Figure 1G-I**). MA plots (expression ratio [M] *vs.* average intensity [A], log transformed) provided an overview of the expression changes of individual genes, revealing that the majority of genes encoding ribosomal proteins (**Figure 2A**), ribosome biogenesis (**Figure 2B**), and translation factors (**Figure 3A**), were enriched in E8.5 neuroepithelium. Expression of ribosomal protein or translation factor genes at E10.5 vs. E8.5 showed a positive correlation (R=0.91 and 0.98 respectively; **Figures 1J, K**), indicating that despite downregulation of most ribosomal and translation factor genes, their stoichiometry remained similar at the two ages. Expression levels of differentially expressed genes at E10.5 vs. E8.5 also showed a positive correlation (R=0.82, **Figure 1L**). There was no correlation between the average expression levels of genes and their fold changes between the two ages (R=-0.1696). Collectively, our data provide transcriptomic signatures of developing forebrain precursors and uncover an overall downregulation of genes encoding protein biosynthetic machinery during the inception of the mammalian forebrain.

Decreased ribosome biogenesis and protein synthesis in E10.5 neuroepithelium

The higher expression of genes associated with ribosomes, ribosome biogenesis, and protein translation in early E8.5 precursors compared to more committed forebrain progenitors at E10.5 suggested that the protein biosynthetic machinery may be differentially regulated during early forebrain development. Ribosomal RNA (rRNA) transcription and initial assembly of pre-ribosomes occurs in nucleoli. As increased ribosome biogenesis is associated with larger nucleoli (Silvera et al., 2010), nucleolar volume provides a proxy for ribosome biogenesis (Baker, 2013; Sanchez et al., 2016). We visualized nucleoli with Fibrillarin (**Figure 2C**), acquired z-stack images of the developing neural tissue, and performed 3D-reconstructions of individual nucleoli in neural precursors (**Figure 2D**). Quantification of nucleolar volume revealed that E8.5 forebrain precursors had larger nucleoli compared to more mature forebrain progenitors at E10.5 (**Figure 2E**). No further reduction in nucleolar volume was observed between E10.5 neuroepithelial cells and E14.5 radial glial progenitors of the cerebral cortex (**Figures 2E**), suggesting that the E8.5 to E10.5 transition represents an important regulatory stage for ribosome biogenesis in the early forebrain.

Focusing on E8.5 and E10.5 neuroepithelia, we observed higher 5.8S pre-rRNA levels in E8.5 vs. E10.5 progenitors by fluorescence in situ hybridization (FISH; **Figure 2F**), and a modest decrease in 5.8S total rRNA at E10.5 (**Figure 2G**) that was supported by Y10b immunostaining (**Figure 2H**). Quantification of 5.8S pre-rRNA signal showed larger nucleolar area in E8.5 progenitors (**Figures 2I, J**), consistent with the fibrillarin quantification (**Figure 2E**). In agreement with these findings, ribosomal proteins including RPL11 and RPS12, which have important roles in the assembly of ribosomal subunits, were more highly expressed at E8.5 vs. E10.5 (**Figures 2K, L;** also Chau et al., 2015). On the other hand, expression of RPL10A protein was similar between the two ages (**Figure 2M**) despite higher *Rpl10a* RNA expression at E8.5

(FPKM: E8.5 = 1962.03; E10.5 = 1242.73), suggesting the involvement of post-transcriptional mechanisms. Transmission electron microscopic (TEM) analyses revealed that E8.5 precursors had more ribosomes than E10.5 progenitors per field of view (**Figure 2N, O**). While ribosome density within the free cytoplasmic space was not different between these two ages (**Figure 2P**), more E10.5 cytoplasm than E8.5 cytoplasm was occupied by other organelles including endoplasmic reticulum, mitochondria, and Golgi (**Figure 2Q**), indicating an overall shift in organelle landscape at this age.

Gene expression analyses demonstrated the parallel downregulation of translational machinery from E8.5 to E10.5 progenitors (**Figure 3A**), including decreased expression of eukaryotic initiation factors (eIFs) such as EIF3η (**Figure 3B**). Activation of the growth promoting mTOR signaling pathway is linked to increased ribosome biogenesis and protein translation, a function mediated by the mTORC1 complex (Laplante and Sabatini, 2012). While mTOR expression was not changed from E8.5 to E10.5 (*Mtor* FPKM: E8.5 = 21.15; E10.5 = 25.91), components of the mTOR signaling pathway were differentially expressed and/or activated at these two ages (**Supplementary File 1**). For example, 4EBP1, a direct target of mTOR, showed increases in both expression and phosphorylation in the E8.5 neuroepithelium (**Figures 3C, D**). S6K1, a direct mTORC1 target that was similarly expressed at the two ages was also more highly phosphorylated at E8.5 compared to E10.5 (**Figure 3E**). Finally, S6 ribosomal protein, a substrate of S6K1, was more highly phosphorylated at E8.5 (**Figures 3F, G**). Taken together, these data demonstrate differential mTOR pathway activation in E8.5 compared to E10.5 neuroepithelium.

E8.5 neural progenitors showed higher ^{35}S-methionine incorporation *in vitro* compared to E10.5 progenitors (counts per million cells, shown as E8.5 fold change normalized to E10.5

progenitors: *Expt. 1 = 2.0-fold; Expt. 2 = 1.4-fold; Expt. 3 = 1.1-fold*), indicative of a higher protein synthesis rate in the younger forebrain progenitor cells. We next visualized actively elongating nascent polypeptides *in vivo* at the single-cell level using O-propargyl-puromycin (OPP; Liu et al., 2012) delivered maternally by intraperitoneal injection (**Figure 3H**). OPP incorporation was higher in E8.5 compared to E10.5 neuroepithelial cell bodies (**Figures 3I, J**), consistent with their larger nucleolar volumes and higher ^{35}S-methionine incorporation. Collectively, these data demonstrate that presumptive forebrain progenitors have higher levels of ribosome biogenesis and protein synthesis compared to more mature progenitor cells of the developing forebrain.

Downregulation of protein biosynthetic machinery matches AF and CSF proteomes

The early developing forebrain is bathed first by amniotic fluid (AF) and following neural tube closure, by cerebrospinal fluid (CSF). As neural progenitors can release signaling factors and membrane particles directly into the CSF (Arbeille et al., 2015; Marzesco et al., 2005), we tested the extent to which the changes observed in the forebrain transcriptome (**Figure 1**) reflected concurrent changes in the AF and CSF proteomes (Chau et al., 2015). We identified 691 proteins present in the AF and CSF that were also expressed by the developing forebrain neuroepithelium. Within this group of 691 proteins, the availability of 493 proteins matched gene expression patterns observed in the forebrain tissue: 395 proteins were enriched in E8.5 AF and more highly expressed by E8.5 neuroepithelium, **Figure 4A**, lower left quadrant; 98 proteins were enriched in E10.5 CSF and more highly expressed by E10.5 neuroepithelium, **Figure 4A,** upper right quadrant. Gene ontology analysis showed that, among proteins and genes enriched in E8.5 AF and neuroepithelium, the most highly represented functional category was

ribosomes/translation (**Figure 4B**). Further analysis revealed that nearly all ribosomal proteins and translation factors were enriched in both E8.5 AF and E8.5 neuroepithelium (**Figures 4C, D**), supporting the model that these fluid proteins can originate in the forebrain tissue. Not only were ribosomal proteins less abundant in E10.5 CSF, but many were no longer detected therein (**Figures 4E;** Chau et al., 2015). Together, these data demonstrate that the changes in the AF and CSF proteomes during early forebrain development match the down-regulation of protein biosynthetic machinery in the adjacent neuroepithelium, thereby providing a developmental biomarker signature of concurrent cell biological changes in the developing forebrain.

MYC modulates ribosome biogenesis in developing forebrain

In other cell types, the transcription factor c-MYC regulates genes encoding ribosomal proteins, proteins involved in ribosome biogenesis, and translation initiation and elongation factors (van Riggelen et al., 2010). Analyses of differentially expressed transcription factors between E8.5 and E10.5 neuroepithelium revealed that *Myc* expression was approximately ten-fold higher in E8.5 neuroepithelium (**Figure 5A**; *Myc* FPKM: E8.5 = 28.73, E10.5 = 2.76), suggesting MYC as a candidate regulator of ribosome biogenesis in the developing forebrain. There was no reciprocal compensatory suppression of *Mycn* or *Mycl* (*Mycn* FPKM: E8.5 = 28.03, E10.5 = 20.91; *Mycl* FPKM: E8.5 = 6.58, E10.5 = 10.34). We confirmed the high level of MYC expression in E8.5 neuroepithelium and its decreased expression in E10.5 neuroepithelium (**Figure 5B, Figure 5-figure supplements 1A-C;** see also Shannon et al., 2018). Once downregulated in E10.5 neural progenitors, MYC expression remained low throughout cerebral cortical development (**Figure 5B**).

GSEA demonstrated that many known MYC target genes were enriched in E8.5 compared to E10.5 neuroepithelium (**Figures 5C, D**; Ben-Porath et al., 2008; Zeller et al., 2003), and some of these target genes were associated with ribosome biogenesis and translation (e.g. *Ncl, Rps13*, and *Eif4e*). To test if interfering with MYC activity regulates ribosome biogenesis, we exposed wild type embryos to the MYC inhibitor, KJ-Pyr-9 (Hart et al., 2014) *in utero*, and observed smaller nucleoli compared to vehicle-injected controls (**Figure 5E**). In agreement with previous studies (Davis et al., 1993; Zinin et al., 2014), we confirmed that *Myc*-deficient embryos showed a triad of developmental defects including smaller size, neural tube closure defects, and developmental delay (**Figure 5-figure supplement 1D**). Nucleolar volume was also decreased in *Myc*-deficient embryos compared to developmentally stage-matched controls (**Figure 5F**).

MYC has important roles in cell cycle regulation (Dang, 2013). Therefore, its rapid downregulation by E10.5 was unexpected given that E10.5 represents a stage of continued progenitor proliferation and the start of forebrain neurogenesis. To determine the consequences of persistent MYC expression on cerebral cortical development, we genetically forced *MYC* expression by crossing StopFLMYC mice (Calado et al., 2012) with *Foxg1-Cre* (Hébert and McConnell, 2000) or *Nestin-Cre* (Tronche et al., 1999) mice (**Figure 5G, Figure 5-figure supplements 1E-G**). We purified Pax6-positive cortical progenitors at E13.5 (from *Nestin-Cre* cross, **Figure 5-figure supplement 1H**), and analyzed gene expression by RNA-seq. We identified 135 differentially expressed genes between WT and MYC-overexpressing (MYC-OE) embryos ($q<0.1$), with 105 genes activated and 30 genes repressed in the MYC-OE progenitors (**Figure 5-figure supplement 1I, Supplementary File 2**). A cross-comparison between the 105 MYC activated genes with our early E8.5-E10.5 RNA-seq dataset (**Figure 1**) revealed 53 genes

that were enriched in E8.5 progenitors when MYC expression is naturally high (**Supplementary File 2).** Functional annotation clustering using DAVID revealed ribosomes as the most enriched gene category among the MYC-upregulated genes (**Figure 5H, Supplementary File 2**). GSEA further revealed that genes encoding ribosome components (**Figure 5I**), genes involved in ribosome biogenesis (**Figure 5J**), along with other known MYC target genes (**Figure 5-figure supplement 1J**; Zeller et al., 2003) were upregulated in the MYC-OE. Among the selective subset of ribosomal proteins that were significantly changed in MYC-OE mice ($q<0.1$), all were upregulated (**Figure 5K, L, Supplementary File 2**), even those subjected to less-stringent statistical significance ($q<0.3$, **Figure 5K**). These gene expression changes were accompanied by a modest increase in ribosome biogenesis in both *Foxg1-Cre* and *Nestin-Cre* MYC-OE mice (**Figure 5 M, N**). Despite this upregulation of ribosome biogenesis and the expression of genes encoding translational machinery (**Figure 5-figure supplement 1K**), changes in protein synthesis at progenitor cell bodies were not consistently observed in either *Myc*-deficient or MYC-OE studies (data not shown). Taken together, these findings demonstrate that *Myc* expression modulates ribosome biogenesis in the developing forebrain, and that additional, as yet unidentified mechanisms participate in the regulation of protein biosynthesis at this developmental stage.

Persistent MYC expression increases progenitor proliferation, leading to macrocephaly

Genes with known functions in regulating cerebral cortical neurogenesis were also upregulated in MYC-OE progenitors including *Insulin-like growth factor 2* (*Igf2*, **Figure 6-figure supplement 1A, Supplementary File 2**), which is typically not highly expressed by apical progenitors and is instead delivered by the CSF to regulate proliferation of progenitors

(Lehtinen et al., 2011), and *Insulinoma-Associated 1* (*Insm1,* **Supplementary File 2**), which accelerates cortical development by promoting delamination of apical progenitor cells (Farkas et al., 2008; Tavano et al., 2018). The coordinated effects of MYC activation of several of these pathways resulted in a large brain phenotype that emerged by E14.5 in both *Foxg1-MYC* and *Nestin-MYC* mice (**Figure 6A-C, Figure 6-figure supplements 1B-D**), and was well defined by birth in *Nestin-MYC* mice (**Figure 6D-G**). No viable pups were recovered from the *Foxg1-Cre* cross (8 litters examined), indicating embryonic lethality between E14.5 and birth. This outcome may be due to the combinatorial effects of MYC overexpression and *Foxg1* heterozygosity (Hébert and McConnell, 2000), perhaps in tissues outside the brain. No differences in body weight were observed at P0 in *Nestin-MYC* mice (body weight [g] ± SEM: WT = 1.35 ± 0.03, n=16; MYC-OE = 1.33 ± 0.02, n=15; unpaired t-test, p=0.57). By P8, MYC-OE and control brains were similar in size (brain weight [g] ± SEM: WT = 0.38 ± 0.01, n=9; MYC-OE = 0.39 ± 0.02, n=6; p=0.72, unpaired t-test). However the MYC-OE mice had much smaller body size (body weight [g] ± SEM: WT = 4.86 ± 0.09, n=13; MYC-OE = 3.20 ± 0.22, n=9; p<0.0001, Welch's t-test), leading to a sustained difference in their brain-body ratio (brain weight/body weight: WT: 0.081 ± 0.001, n=9; MYC-OE: 0.127 ± 0.006, n=6; p=0.0003, Welch's t-test).

While no tumors were observed at the ages examined in this study, histological analyses suggested that MYC-OE by the *Nestin* promoter increased the size of the entire brain. A two-hour BrdU pulse delivered at E15.5 showed a larger proportion of Pax6-positive apical progenitors in S-phase in MYC-OE mice (**Figure 6H**), contributing to increased cortical thickness in MYC-OE mice by birth (**Figure 6I, J**). MYC-OE cortices had increased Cux1-positive staining cells destined for the upper layers of the cerebral cortex (**Figure 6K, L**), which contributed to the increased overall number of cells in the cerebral cortex (cell number ± SEM:

WT: 2,348 ± 199.3; MYC-OE: 2,518 ± 174.3, n=4, p=0.07, paired t-test). On the other hand, no difference was observed in the number of Ctip2-positive lower layer neurons (cell number ± SEM: WT: 651.5 ± 35.4; MYC-OE: 639 ± 34.9, n=4, p=0.82, paired t-test). Together, our findings support the model that MYC overexpression in the *Nestin* lineage affects multiple pathways and that their convergence influences the development of the brain and the entire organism.

DISCUSSION

Our study reveals major changes in expression of the protein biosynthetic pathway during early specification of the mammalian forebrain. This work (1) demonstrates that enhanced biogenesis of ribosomes and protein synthetic machinery serve as transcriptional and cell biological signatures defining early forebrain precursor cells; (2) reveals that the changing proteomes of AF and CSF provide a biomarker signature that matches the concurrent, normal development of the adjacent forebrain; (3) identifies MYC as a contributor to the regulation of ribosome biogenesis in the developing forebrain; and (4) shows that persistent MYC expression leads to increased ribosome biogenesis, enhanced cortical progenitor proliferation, and macrocephaly. We conclude that, as in other stem cells, neural progenitor cells dynamically regulate protein biosynthetic machinery to meet their changing needs, and that this process is regulated in part by MYC.

The DNA transcriptome is an essential starting point for our understanding of tissue regionalization, patterning, and individual cell identities in the mammalian central nervous system. Nevertheless, not all mRNAs are selected for protein translation, and our discovery of temporal regulation of the protein biosynthetic machinery during early specification of the forebrain uncovers a new layer of regulation fundamental to the early construction of the brain. Regulation of the protein biosynthetic machinery provides a tunable molecular program harnessed by cells to guide transitions between stem cell states (DeBoer et al., 2013; Fujii et al., 2017; Khajuria et al., 2018; Kraushar et al., 2016; Sanchez et al., 2016; Scognamiglio et al., 2016). Cell cycle in the forebrain lengthens over the course of development (Caviness and Takahashi, 1995). As such, the higher rates of ribosome biogenesis and protein synthesis observed in neurectodermal precursors relative to post-neurulation progenitors are consistent

with a model in which rapidly dividing cells synthesize more proteins to support their proliferation (Buszczak et al., 2014). Genes such as *Pelo* and *Abce1* are downregulated in E10.5 progenitors (**Supplementary File 1**), suggesting that additional levels of translational control including ribosome recycling may be engaged during this developmental time window (Dever and Green, 2012).

Disruptions in ribosome structure and function are linked to a number of genetically inherited ribosomopathies such as Diamond-Blackfan anemia (Boria et al., 2010; Choesmel et al., 2007; Ebert and Lipton, 2011). Nucleolar size, ribosome biogenesis, and protein translation have been implicated in aging and longevity (Buchwalter and Hetzer, 2017; Tiku et al., 2016). In the central nervous system, disruptions in mRNA processing and translation can eventually impair the form and function of delicate neural circuitry. Changes in mRNA binding proteins are linked to neurodevelopmental disorders including autism spectrum disorder (Kraushar et al., 2014; Popovitchenko et al., 2016), and stem cell-derived neural progenitors from schizophrenia patients have altered levels of protein synthesis (Topol et al., 2015). During later stages of neurogenesis in the cerebral cortex, subcellular transport of mRNA by binding proteins including FMRP (Fragile-X mental retardation protein) ferry mRNA to sites of local translation in more polarized cells (Kwan et al., 2012; Pilaz et al., 2016; Pilaz and Silver, 2017). It is tempting to speculate that in the developing forebrain, the assembly of specialized ribosomes could enable unique or localized translation in developing precursor cells, fine-tuning cellular identities and tailoring individualized developmental programs as in other tissues (Bortoluzzi et al., 2001; Fujii et al., 2017; Shi et al., 2017; Simsek et al., 2017).

While ribosomal protein expression and ribosome biogenesis decrease as the embryo develops, we did not observed any difference in cytoplasmic ribosome density from EM analysis

(**Figure 2**). This might be due to the long half-life of ribosomes (Hirsch & Hiatt, 1966; Nikolov et. al., 1983), and thus ribosomes generated earlier at E8.5 would likely still be present at E10.5. Using OPP and methionine incorporation, we provided evidence that protein synthesis is also downregulated as the embryo develops. However, we do not know whether differential protein synthesis is driven by changes in ribosome biogenesis or by overall changes in transcription dynamics. Furthermore, OPP was administered intraperitoneally into the pregnant dams, and it is possible that availability of OPP to the embryonic progenitors might be different between E8.5 and E10.5. Indeed, increased ribosomal protein expression does not always result in increased translation because not all ribosomal proteins are associated with polysomes (Kraushar et al., 2015). It is possible that some ribosomal proteins perform extraribosomal functions independent of translation (Warner & Mclntosh, 2009; Zhou et al., 2015). For instance, RPL11 is recruited to the promoter regions of p53 target genes during nucleolar stress to promote p53 transcriptional activity (Mahata et al., 2012). Therefore, additional evidence is needed to confirm that changes in ribosome biogenesis directly cause differential protein synthesis in the early neural progenitors.

Neural progenitors depend on their adjacent fluid environment for appropriate fluid pressure and instructive signals (Lun et al., 2015). Developing neural tissue also releases membrane bound vesicles into the adjacent fluid environment (Cossetti et al., 2014; Marzesco et al., 2005). We found that the protein biosynthetic changes occurring in the forebrain neuroepithelium were reflected in the proteomic content of the adjacent AF and CSF (**Figure 4**). The CSF is commonly sampled for biomarkers of neurologic diseases. Our data demonstrate that during early forebrain development, the proteomic signature of the early brain fluids provides a biomarker signature of the normal, healthy forebrain, opening a new “window” into this stage of

early brain development. Whether the ribosomal and translational machinery found in the AF and CSF are equipped to actively synthesize proteins within the fluid environment remains to be elucidated. Alternatively, the fluids might serve as a channel for intercellular transfer of ribosomes and other proteins (Cossetti et al., 2014; Court et al., 2008). Future studies will also reveal whether maturation-associated, release of protein biosynthetic machinery into the developing brain fluids is an active or passive process, and whether this process shares features with membrane shedding that occurs in other cell types, such as at the maturing red blood-cell surface (Gautier et al., 2016).

The swift downregulation of MYC following neurulation could be due to chromatin modifications, epigenetic mechanisms, and/or inhibition of RNA polymerase II elongation. *Myc*-deficiency (Kerosuo and Bronner, 2016) as well as ground-level changes in DNA methylation, histone modifications, and nucleosome positioning are associated with NTD (reviewed in Greene and Copp, 2014; Wilde et al., 2014). Cross-referencing our data (**Figure 1**) with NTD Wiki, a repository of genes required for neurulation (www.ntdwiki.wikispaces.com), revealed that a number of MYC targets are associated with NTD (data not shown). Complex gene-environment interactions have long been appreciated to underlie NTD. Despite modern successes in reducing the incidence of NTD by dietary fortification (e.g. folate) and increased awareness of adverse consequences of maternal exposures (e.g. alcohol and drug use) on the developing fetus, NTD continue to represent one of the most common birth defects worldwide (Wallingford et al., 2013). Neurulation varies along the anterior-posterior axis, and specific cell types (e.g. hinge points, neural fold cells) have distinct roles in this process (Massarwa et al., 2014). Thus, while our study investigated anterior forebrain development, variation in expression of the protein biosynthetic machinery along the anterior-posterior and dorsal-ventral/medial-lateral axes could

differentially affect neurulation along the entire body axis. Overall, the identification of molecular pathways regulating protein biosynthetic machinery during neurulation may provide new opportunities to seek answers to these complex conditions.

Aberrant regulation of the signaling pathways examined in this study in cortical progenitors are associated with cortical overgrowth syndromes such as hemimegalencephaly, a brain malformation characterized by unilateral enlargement of one hemisphere (D'Gama et al., 2017; Poduri et al., 2012). Increased *MYC* expression has been reported in hemimegalencephaly (Yu et al., 2005), though to our knowledge, mutations in *MYC* itself have not been shown to drive the pathogenesis of this malformation.

While perhaps best known for its role as an oncogene, we did not observe any cortical tumors in *Nestin:MYC* brains. Context-dependent effects of MYC have been reported, with age- and tissue-dependent effects on cellular phenotypes including proliferation and cell growth (Gabay et al., 2014; Zinin et al., 2014). The tumorigenic consequences of persistent *MYC* expression of this model emerged later in adult mice as choroid plexus carcinoma and ciliary body medulloepithelioma (Shannon et al., 2018), exposing the select vulnerability of certain subtypes of epithelial cells in the *Nestin* lineage to tumorigenesis. Such selectivity of MYC-associated pathologies may be determined by the epigenetic landscape of differentiated cells in adult tissues. MYC may act as a universal amplifier of expressed genes, promoting proliferation in already dividing cells (Lin et al., 2012; Nie et al., 2012). However, in more differentiated cells, genes may be confined to heterochromatin and inaccessible to MYC (Kress et al., 2015). Certain cell types may also require a genetic double-hit such as concomitant *p53*-deficiency in the cortex (Momota et al., 2008), or particular gene-environment triggers, for transformation.

Overall, cellular identity and health reflect the net equation between a cell's transcriptional and translational output (Buszczak et al., 2014; Fujii et al., 2017; Holmberg and Perlmann, 2012; Khajuria et al., 2018; Sanchez et al., 2016). These processes require multiple regulatory steps that are vulnerable to disruptions accumulating from cell-intrinsic genetic programs, and/or cell-extrinsic environmental cues. In the developing brain, environmental signals can entail disturbances of local gradients diffusing through tissues (e.g. Toyoda et al., 2010) or altered delivery of growth-promoting factors by the adjacent AF or CSF (Chau et al., 2015; Lehtinen et al., 2011). All of these signaling activities are susceptible to exogenous maternal exposures including illness, substance abuse, and environmental toxins. Thus, our findings provide a new paradigm for understanding brain development through investigation of molecular pathways regulating the biosynthetic machinery in forebrain progenitors.

MATERIALS AND METHODS

Key Resources Table

Reagent type (species) or resource	Designation	Source or reference	Identifiers	Additional information
strain, strain background (*Mus Musculus*)	Gt(ROSA)26Sor$^{tm13(CAG-MYC,-CD2*)Rsky}$ (referred as StopFLMYC)	The Jackson Laboratory	MGI:5444670	Maintained on a C57Bl/6 background
strain, strain background (*Mus Musculus*)	Tg(Nes-cre)1Kln (referred as Nestin-cre)	The Jackson Laboratory	MGI:2176173	Maintained on a C57Bl/6 background
strain, strain background (*Mus Musculus*)	Foxg1$^{tm1(cre)Skm}$ (referred as Foxg1-cre)	The Jackson Laboratory	MGI:1932522	Maintained on a C57Bl/6 background
strain, strain background (*Mus Musculus*)	Myc-deficient mice (c-myc$^{-/-}$)	Provided by Troy Baudino	Baudino et al., Genes Dev., 2002	Maintained on a C57Bl/6 background
strain, strain background (*Mus Musculus*)	CD-1 IGS Mouse (referred as CD-1)	Charles River	Strain code: 022	Wildtype timed pregnant mice
antibody	Rabbit anti-4E-BP1	Cell Signaling	9644	1:1000
antibody	Mouse anti-5.8S ribosomal RNA [Y10B]	Abcam	ab171119	1:50; antigen retrieval with steaming in citric acid
antibody	Mouse anti-ACTB	Cell Signaling	12262	1:2000
antibody	Rat anti-BrdU	Biorad	MCA2060	1:200; antigen retrieval with steaming in citric acid
antibody	Rabbit anti-MYC	Abcam	ab32072	1:100 for IHC, antigen retrieval with steaming in citric acid; 1:2000 for WB
antibody	Rat anti-CTIP2	Abcam	ab18465	1:200
antibody	Rabbit anti-CUX1	Santa Cruz Biotechnology	sc13024	1:200
antibody	Mouse anti-EIF3η	Santa Cruz Biotechnology	sc137214	1:100; antigen retrieval with steaming in citric acid
antibody	Mouse anti-Fibrillarin	Abcam	ab4566	1:250; antigen retrieval with steaming in citric acid
antibody	Mouse anti-GAPDH	Cell Signaling	97166	1:1000
antibody	Rabbit anti-p4E-BP1	Cell Signaling	2855	1:200 for IHC; 1:1000 for WB
antibody	Rabbit anti-PAX6	Biolegend	901301	1:100; antigen retrieval with steaming in citric acid; 1:1000 for FACS
antibody	Rabbit anti-pS6	Cell Signaling	5364	1:200 for IHC; 1:1000 for WB
antibody	Rabbit anti-pS6K	Cell Signaling	9234	1:1000
antibody	Mouse anti-pVimentin	Enzo Bioscience	ADI-KAM-CC249-E	1:400
antibody	Mouse anti-RPL10A	Novusbio	H00004736-M01	1:500
antibody	Rabbit anti-RPL11	Santa Cruz Biotechnology	sc50363	1:50
antibody	Rabbit anti-RPS12	Proteintech	16490-1-AP	1:50
antibody	Rabbit anti-S6	Cell Signaling	2217	1:1000
antibody	Rabbit anti-S6K	Cell Signaling	9202	1:1000
antibody	Mouse anti-TUJ1	Biolegend	801202	1:100 for IHC; 1:1000 for FACS
antibody	Rabbit anti-Vinculin	Cell Signaling	13901	1:1000
Recombinant DNA reagent	Quaser 570 coupled 5.8S pre-rRNA FISH probe	Provided by Debra Silver		1:200
Recombinant DNA reagent	Quaser 670 coupled 5.8S total rRNA FISH probe	Provided by Debra Silver		1:200

commercial assay or kit	RecoverAll Total Nucleic Acid Isolation Kit for FFPE	Ambion	AM1975	Manufacturer's protocol
commercial assay or kit	Ovation RNA-Seq System V2	Nugen	7102	Manufacturer's protocol
commercial assay or kit	Ovation Ultralow System V2 1-16	Nugen	0344	Manufacturer's protocol
commercial assay or kit	TruSeq RNA Library Prep Kit v2	Illumina	RS-122	Manufacturer's protocol
commercial assay or kit	Rneasy Micro Kit	Qiagen	74004	Manufacturer's protocol
commercial assay or kit	Pierce™ BCA Protein Assay Kit	Thermo Fisher Scientific	23227	
commercial assay or kit	Click-iT plus OPP protein synthesis assay kit	Thermo Fisher Scientific	C10456	
chemical compound, drug	O-propargyl-puromycin (OPP)	Life Technologies	C10459	IP injection, dosage: 50mg/kg
chemical compound, drug	KJ-Pyr-9	Tocris	5306	IP injection, dosage: 10mg/kg
chemical compound, drug	^{35}S-Methionine	Perkin Elmer	NEG709A	51µCi
chemical compound, drug	5-Bromo-2′-deoxyuridine (BrdU)	Sigma	B5002	IP injection, 50mg/kg
software, algorithm	TopHat	https://ccb.jhu.edu/software/tophat/index.shtml	v2	RNAseq analysis
software, algorithm	Cufflinks	http://cole-trapnell-lab.github.io/cufflinks/	v2	RNAseq analysis
software, algorithm	DAVID	https://david.ncifcrf.gov/	v6.7, 6.8	RNAseq analysis
software, algorithm	GSEA	http://software.broadinstitute.org/gsea/index.jsp	v2	RNAseq analysis
software, algorithm	R Studio	Rstudio, Inc.	v0.99	RNAseq analysis
software, algorithm	Prism	GraphPad	v7	Statistical analysis
software, algorithm	FIJI (Image J)	https://fiji.sc/#	v1	Image analysis
software, algorithm	Imaris	Bitplane		Image analysis

Mice

Timed pregnant CD1 dams were obtained from Charles River Laboratories. *Myc*-deficient mice (Baudino et al., 2002) were maintained in a C57BL/6J genetic background. StopFLMYC mice (JAX: 020458) were maintained in a C57BL/6J genetic background and crossed with *Nestin-cre* line (JAX: 003771) or *Foxg1-cre* line (JAX: 004337) to generate MYC-OE mice, in which human *MYC* transgene is selectively expressed in neural progenitor cells. All analyses were carried out using male and female mice. All animal experimentation was carried out under protocols approved by the IACUC of Boston Children's Hospital.

E8.5 and E10.5 forebrain epithelium RNAseq

Forebrain epithelium at E8.5 and E10.5 was dissected as described (Chau et al., 2015). Each sequenced sample comprised forebrain epithelial tissues pooled across one litter. Total RNA was isolated using the RNeasy Micro Kit (Qiagen), converted to cDNA, and preamplified using the Ovation RNA-seq System V2 (NuGEN) following the manufacturer's instructions. cDNA was converted to Illumina paired-end sequencing libraries following the standard protocol (TruSeq v2) and sequenced on a Illumina HiSeq 2000 instrument to a depth of ~20–60 million pass-filter reads per library, after standard quality control filters. The 50 base pair paired-end reads were mapped to the UCSC mm9 mouse reference genome using TopHat v2, and fragments per kilobase per million reads (FPKM) values were estimated using cufflinks v2, and differentially expressed genes (DEG) were identified using cuffdiff v2 with q value < 0.05 (Trapnell et al., 2012).

FACS of neural progenitors

E13.5 dorsal telencephalon was microdissected, avoiding the lateral ganglionic eminence and structures ventral to it. The cortex was separated from the meninges, and cortices from samples of the same genotype were pooled and sliced into small, uniformly sized pieces. Tissues were digested with 2.5% Trypsin (Invitrogen), then dissociated into single cells by repeated pipetting. Cells were fixed in 4% PFA, incubated with primary antibodies, and then secondary antibodies. Each step was carried out in 4°C for 30 mins, with rotation. RNAsin (NEB) was added to buffers to prevent RNA degradation (Hrvatin et al., 2014). Cells were sorted using FACS Aria IIU (BD). Antibodies: Rabbit anti-PAX6 (Biolegend 901301, 1:1000), Mouse anti-TUJ1 (Biolegend 801202, 1:1000)

506

507 E13.5 neural progenitor RNAseq

508 RNA was extracted from sorted neural progenitors using RecoverAll Total Nucleic Acid
509 Isolation Kit (Ambion), then reverse transcribed into cDNA and pre-amplified using Ovation
510 RNA-Seq System V2 (Nugen 7102). Libraries were prepared using Ovation Ultralow System V2
511 1-16 (Nugen 0344), and sequenced (Illuminia HiSeq 2500) to a depth of ~25-40 million reads
512 per library. The 50 base pair single-end reads were mapped to the UCSC mm10 mouse reference
513 genome using TopHat v2, FPKM values were estimated using cufflinks v2, and DEG were
514 identified using cuffdiff v2 with q value < 0.1 (Trapnell et al., 2012).

515

516 RNAseq data analysis

517 All analyses were performed using genes with FPKM > 1, which we considered as the threshold
518 of expression. Hierarchical clustering and heatmaps of differentially expressed genes were
519 generated in R using the heatmap.2 command in 'gplots' package, FPKM values were log2
520 transformed, and centered and scaled by rows for display purposes. Distance was calculated
521 using the 'Maximum' method whereas clustering was performed using the 'Complete' method.
522 Functional annotation clustering was performed using DAVID v6.7 and v6.8
523 (https://david.ncifcrf.gov/home.jsp; Huang et al., 2009). Gene set enrichment analysis was
524 performed using GSEA v2 Subramanian et al., 2005), gene sets were obtained from the Broad
525 Institute Molecular Signatures Database (http://software.broadinstitute.org/gsea/msigdb). MA
526 plots were created in R using the ma.plot command in the 'affy' package, and MS vs RNAseq
527 plots were created using the plot command.

528

Tissue processing

Samples were fixed in 4% paraformaldehyde (PFA). For cryosectioning, samples were incubated in the following series of solutions: 10% sucrose, 20% sucrose, 30% sucrose, 1:1 mixture of 30% sucrose and OCT (overnight), and OCT (1 hour). Samples were frozen in OCT. For microtome sectioning, samples were paraffin embedded in the histology core at Beth Israel Deaconess Medical Center.

Immunohistochemistry

Cryosections were blocked and permeabilized (0.3% Triton-X-100 in PBS; 5% serum), incubated in primary antibodies overnight and secondary antibodies for 2 hours. Sections were counterstained with Hoechst 33342 and mounted using Fluoromount-G (SouthernBiotech). The following primary antibodies were used: anti-5.8S rRNA (Y10b; Abcam, ab171119, 1:50), anti-BrdU (Biorad, MCA2060, 1:200), anti-cMYC (Abcam, ab32072, 1:100), anti-CTIP2 (Abcam, ab18465, 1:200), anti-Cux1 (Santa Cruz Biotechnology, sc13024, 1:200), anti-EIF3η (Santa Cruz Biotechnology, sc-137214, 1:100), anti-Fibrillarin (Abcam, ab4566, 1:250), anti-p4E-BP1 (Cell Signaling, 2855, 1:200), anti-Pax6 (Biolegend, 901301, 1:100), anti-pS6 (Cell Signaling, 5364, 1:200), anti-pVimentin (Enzo Bioscience, ADI-KAM-CC249-E, 1:400), anti-Rpl11 (Santa Cruz Biotechnology, sc50363 1:50), anti-Rps12 (Proteintech, 16490-1-AP, 1:50), anti-Tuj1 (Biolegend, 801202, 1:100). Secondary antibodies were selected from the Alexa series (Invitrogen, 1:500). For BrdU, Fibrillarin, Pax6, cMyc, 5.8S rRNA, and EIF3η staining, antigen retrieval/denaturation was performed before the blocking step: A food steamer (Oster 5712) was filled with water and preheated until the chamber was approximately 100°C, sections were immersed in boiling citric acid buffer (10mM sodium citrate; 0.05% Tween 20; pH=6) and

552 placed in steamer for 20 minutes. Sections were cooled to room temperature. H&E staining was
553 carried out according to standard procedures (Shannon et al., 2018).
554
555 Immunoblotting
556 Tissues were homogenized in RIPA buffer supplemented with protease and phosphatase
557 inhibitors. Protein concentration was determined by BCA assay (Thermo Scientific 23227).
558 Samples were denatured in 2% SDS by heating at 95°C for 5 minutes. Equal amounts of proteins
559 were loaded and separated by electrophoresis in a 4-15% gradient polyacrylamide gel,
560 transferred to nitrocellulose blot (250mA, 1.5 hours), blocked in 5% BSA or milk, incubated
561 with primary antibodies overnight at 4°C followed by HRP conjugated secondary antibodies
562 (1:5000) for 1 hour, and visualized with ECL substrate. For phosphorylation analysis, the
563 phospho-proteins were probed first, and then blots were stripped (Thermo Scientific 21059) and
564 reprobed for total proteins. The following primary antibodies were used: anti-4E-BP1 (Cell
565 Signaling, 9644, 1:1000), anti-ACTB (Cell Signaling, 12262, 1:2000), anti-cMYC (Abcam,
566 ab32072, 1:2000), anti-GAPDH (Cell Signaling, 97166, 1:1000), anti-p4E-BP1 (Cell Signaling,
567 9459, 1:1000), anti-pS6 (Cell Signaling, 5364, 1:1000), anti-pS6K (Cell Signaling, 9234, 1:1000),
568 anti-RPL10A (Novusbio, H00004736-M01, 1:500), anti-S6 (Cell Signaling, 2217, 1:1000), anti-
569 S6K (Cell Signaling, 9202, 1:1000), anti-Vinculin (Cell Signaling, 13901, 1:1000).
570
571 Fluorescent in situ hybridization
572 Cryosections were permeabilized in 0.5% Triton-X-100 for 20 minutes, incubated with probes
573 (Pilaz et al., 2016) overnight at 37°C, counterstained with Hoechst, and mounted using

Fluoromount-G (SouthernBiotech). Probes: Quaser 570 coupled 5.8S pre-rRNA, Quaser 670 coupled 5.8S total rRNA.

^{35}S-Methionine labeling

E8.5 and E10.5 forebrain neuroepithelium was dissected as described (Chau et al., 2015) and trypsinized. Cells were serum starved in methionine-free DMEM for 1 hour at 37°C, then incubated with 51μCi ^{35}S-Methionine (Perkin Elmer NEG709A) at 37°C for an additional hour. Cycloheximide (50μg/ml) was added to stop translation. ^{35}S-Methionine incorporation was measured using scintillation counter.

Nucleolar volume quantification

Nucleolar volume was quantified according to published methods using Imaris (Bitplane; Baker, 2013; Sanchez et al., 2016; Shannon et al., 2018; Silvera et al., 2010). To ensure fair representation, randomly selected nucleoli were selected for quantification across the image field. When quantifying nucleolar volume embryonically, we specifically quantified cells close to the ventricular surface. Therefore, at E14.5 the quantified cells should represent radial glia in the ventricular zone. For relative nucleolar volume, each volume value was normalized to the average nucleolar volume of the controls in the corresponding litter. 5.8S rRNA signal area (nucleolar area) was quantified using FIJI (Image J).

Neuroepithelium OPP quantification

OPP quantification was performed as described by Liu et al. (2012). Pregnant dams received intraperitoneal OPP injections (50 mg/kg OPP; Life Technologies). One hour later, developing

597 tissues were obtained and sectioned to a thickness of 7 μm using a cryostat. OPP signals were
598 detected using the Click-iT plus OPP protein synthesis assay kits (Life Technologies) according
599 the manufacturer's suggested procedures. Images were taken at 20X (Zeiss Axio Observer D1
600 inverted microscope) and fluorescence intensity was quantified using FIJI (ImageJ). For each
601 sample, OPP intensity from 6 independent regions of interest (185 μm^2) along the ventricular
602 surface was measured and averaged.
603
604 MYC inhibitor injection
605 KJ-Pyr-9 (Hart et al., 2014) was dissolved in Tween 80:DMSO:5% dextrose (1:1:8) and injected
606 at a dosage of 10mg/kg into pregnant dams at E7.5. Samples were collected 24 hours later for
607 analysis.
608
609 BrdU cell proliferation assay
610 BrdU (50mg/kg) was injected intraperitoneally into pregnant dams 2 hours prior to tissue
611 collection. Brains were cryosectioned (7 μm thickness) and stained with BrdU and Pax6
612 antibodies. Images were acquired at 20X (Zeiss LSM 700 laser scanning confocal microscope).
613 Cells were counted in a 100 μm wide column in the dorsal-lateral cortex. For each sample, 4 – 6
614 sections along the anterior/posterior axis of the forebrain were counted and averaged. The
615 proliferation index was defined as the percentage of Pax6-positive cells that were also BrdU-
616 positive.
617
618 P0 cortical neuron counting

14 μm thick cryosections were stained with antibodies, and images were acquired at 20X (Zeiss Axio Observer D1 inverted microscope). Counting was performed using FIJI (Image J) on 100 μm wide columns in the dorsal-lateral cortex in the region just anterior to the hippocampus.

P0 cortical thickness measurement

Measurements were performed on H&E-stained coronal sections. Thickness was defined as the length extending from the ventricular zone up to the pial surface in the dorsal-lateral cortex.

Quantitative RT-PCR

RNA was isolated using Trizol extraction protocol or RecoverAll Total Nucleic Acid Isolation Kit (Ambion), and reverse-transcribed into cDNA. Gene expression was measured by Taqman qPCR (Life Technologies), using *Tbp* as an internal control.

Transmission Electron Microscopy

All tissue processing, sectioning, and imaging was carried out at the Conventional Electron Microscopy Facility at Harvard Medical School. E8.5 and E10.5 tissues were fixed in 2.5% Glutaraldehyde/2% Paraformaldehyde in 0.1 M sodium cacodylate buffer (pH 7.4). They were then washed in 0.1M cacodylate buffer and postfixed with 1% Osmiumtetroxide (OsO4)/1.5% Potassiumferrocyanide (KFeCN6) for one hour, washed in water three times and incubated in 1% aqueous uranyl acetate for one hour. This was followed by two washes in water and subsequent dehydration in grades of alcohol (10 minutes each; 50%, 70%, 90%, 2x10min 100%). Samples were then incubated in propyleneoxide for one hour and infiltrated overnight in a 1:1 mixture of propyleneoxide and TAAB Epon (Marivac Canada Inc. St. Laurent, Canada). The following day,

642 the samples were embedded in TAAB Epon and polymerized at 60 degrees C for 48 hours.
643 Ultrathin sections (about 80nm) were cut on a Reichert Ultracut-S microtome, and picked up
644 onto copper grids stained with lead citrate. Sections were examined in a JEOL 1200EX
645 Transmission electron microscope or a TecnaiG² Spirit BioTWIN. Images were recorded with an
646 AMT 2k CCD camera.

647 Ribosomal quantification was performed using Imaris (Bitplane). For 20 images per
648 individual (N=3 at each age), ribosomal density was calculated within a 280.5nm x 280.5nm box
649 in an inverted color image that contained only cytoplasm and ribosomes (no membrane bound
650 organelles). Ribosomes were counted by the Imaris software using the "spots" tool, with
651 estimated diameter of 250px and with automatic background subtraction "on", and quality above
652 the automatic threshold. The number of ribosomes per field of view (FOV) was calculated by
653 multiplying the above calculate density by the cytoplasmic area. The cytoplasmic area was
654 calculated by creating a hand-drawn surface in Imaris around the free cytoplasmic space in the
655 standard FOV (2692nm x 1762.6 nm). The % FOV occupied by organelles was calculated by
656 subtracting the free cytoplasmic area from the total area to arrive at the organelle-occupied area.
657

658 Statistical Analysis

659 Biological replicates (N) were defined as samples from distinct individuals analyzed either in the
660 same experiment or within multiple experiments. Samples were pooled across multiple litters so
661 as to reduce inter-litter variability. Statistical analyses were performed using Prism 7 or R.
662 Outliers were excluded using ROUT method (Q = 1%). Appropriate statistical tests were selected
663 based on the distribution of data, homogeneity of variances, and sample size. F tests or Bartlett's
664 tests were used to assess homogeneity of variances between data sets. Parametric tests (T test,

ANOVA) were used only if data were normally distributed and variances were approximately equal. Otherwise, nonparametric alternatives were chosen. Data are presented as means ± standard errors of the mean (SEMs). Please refer to figure legends for statistical tests used and sample size. P values < 0.05 were considered significant (*P≤0.05, **P≤0.01, ***P≤0.001, ****P≤0.0001)

ACKNOWLEDGEMENTS

We thank members of the Lehtinen and Fleming labs, C. Harwell, A. LaMantia, S. Dymecki, A. Lassar, and R. Segal for helpful discussions, T. Baudino for *Myc* knockout mice, D. Silver for FISH probes, J. Steen for RPS12 and RPL11 antibodies, M. Baizabal, M. Ericsson, A. Malesz, and P. Schmidt for experimental advice and assistance. We are grateful for the following support: NSF Graduate Research Fellowship (KFC), NIH T32 HL110852 (KFC and RMF), Pediatric Hydrocephalus Foundation, Simons Foundation SFARI Pilot Grant, NIH R01 NS088566 (MKL), BCH IDDRC 1U54HD090255, and the New York Stem Cell Foundation. M.K. Lehtinen is a New York Stem Cell Foundation – Robertson Investigator.

COMPETING INTERESTS

The authors declare that no competing interests exist.

720 **REFERENCE**
721

722 Arbeille, E., Reynaud, F., Sanyas, I., Bozon, M., Kindbeiter, K., Causeret, F., Pierani, A., Falk,
723 J., Moret, F., and Castellani, V. (2015). Cerebrospinal fluid-derived Semaphorin3B orients
724 neuroepithelial cell divisions in the apicobasal axis. Nature communications *6*, 6366.

725 Baker, N.E. (2013). Developmental regulation of nucleolus size during Drosophila eye
726 differentiation. PloS one *8*.

727 Baudino, T.A., McKay, C., Pendeville-Samain, H., Nilsson, J.A., Maclean, K.H., White, E.L.,
728 Davis, A.C., Ihle, J.N., and Cleveland, J.L. (2002). c-Myc is essential for vasculogenesis and
729 angiogenesis during development and tumor progression. Genes & development *16*, 2530-2543.

730 Ben-Porath, I., Thomson, M.W., Carey, V.J., Ge, R., Bell, G.W., Regev, A., and Weinberg, R.A.
731 (2008). An embryonic stem cell-like gene expression signature in poorly differentiated
732 aggressive human tumors. Nature genetics *40*, 499-507.

733 Bjornsson, C.S., Apostolopoulou, M., Tian, Y., and Temple, S. (2015). It Takes a Village:
734 Constructing the Neurogenic Niche. Developmental cell *32*, 435-446.

735 Boria, I., Garelli, E., Gazda, H.T., Aspesi, A., Quarello, P., Pavesi, E., Ferrante, D., Meerpohl,
736 J.J., Kartal, M., Da Costa, L.*, et al.* (2010). The ribosomal basis of Diamond-Blackfan Anemia:
737 mutation and database update. Human mutation *31*, 1269-1279.

738 Bortoluzzi, S., d'Alessi, F., Romualdi, C., and Danieli, G.A. (2001). Differential expression of
739 genes coding for ribosomal proteins in different human tissues. Bioinformatics (Oxford,
740 England) *17*, 1152-1157.

741 Buchwalter, A., and Hetzer, M.W. (2017). Nucleolar expansion and elevated protein translation
742 in premature aging. Nat Commun *8*, 328.

743 Buszczak, M., Signer, R.A., and Morrison, S.J. (2014). Cellular differences in protein synthesis
744 regulate tissue homeostasis. Cell *159*, 242-251.

745 Calado, D., Sasaki, Y., Godinho, S.A., Pellerin, A., Köchert, K., Sleckman, B.P., de Alborán, I.,
746 Janz, M., Rodig, S., and Rajewsky, K. (2012). The cell-cycle regulator c-Myc is essential for the
747 formation and maintenance of germinal centers. Nature immunology *13*, 1092-1100.

748 Caviness, V.S., and Takahashi, T. (1995). Proliferative events in the cerebral ventricular zone.
749 Brain & development *17*, 159-163.

750 Chau, K.F., Springel, M.W., Broadbelt, K.G., Park, H.-Y.Y., Topal, S., Lun, M.P., Mullan, H.,
751 Maynard, T., Steen, H., LaMantia, A.S.*, et al.* (2015). Progressive Differentiation and Instructive
752 Capacities of Amniotic Fluid and Cerebrospinal Fluid Proteomes following Neural Tube
753 Closure. Developmental cell *35*, 789-802.

754 Choesmel, V., Bacqueville, D., Rouquette, J., Noaillac-Depeyre, J., Fribourg, S., Crétien, A.,
755 Leblanc, T., Tchernia, G., Da Costa, L., and Gleizes, P.-E.E. (2007). Impaired ribosome
756 biogenesis in Diamond-Blackfan anemia. Blood *109*, 1275-1283.

757 Cossetti, C., Iraci, N., Mercer, T.R., Leonardi, T., Alpi, E., Drago, D., Alfaro-Cervello, C., Saini,
758 H.K., Davis, M.P., Schaeffer, J.*, et al.* (2014). Extracellular Vesicles from Neural Stem Cells

759 Transfer IFN-γ via Ifngr1 to Activate Stat1 Signaling in Target Cells. Molecular Cell *56*, 193-
760 204.

761 Court, F.A., Hendriks, W.T., MacGillavry, H.D., Alvarez, J., and van Minnen, J. (2008).
762 Schwann cell to axon transfer of ribosomes: toward a novel understanding of the role of glia in
763 the nervous system. J Neurosci *28*, 11024-11029.

764 D'Gama, A.M., Woodworth, M.B., Hossain, A.A., Bizzotto, S., Hatem, N.E., LaCoursiere, C.M.,
765 Najm, I., Ying, Z., Yang, E., Barkovich, A.J.*, et al.* (2017). Somatic Mutations Activating the
766 mTOR Pathway in Dorsal Telencephalic Progenitors Cause a Continuum of Cortical Dysplasias.
767 Cell Rep *21*, 3754-3766.

768 Dang, C.V. (2013). MYC, metabolism, cell growth, and tumorigenesis. Cold Spring Harb
769 Perspect Med *3*.

770 Davis, A.C., Wims, M., Spotts, G.D., Hann, S.R., and Bradley, A. (1993). A null c-myc mutation
771 causes lethality before 10.5 days of gestation in homozygotes and reduced fertility in
772 heterozygous female mice. Genes & development *7*, 671-682.

773 DeBoer, E.M., Kraushar, M.L., Hart, R.P., and Rasin, M.R. (2013). Post-transcriptional
774 regulatory elements and spatiotemporal specification of neocortical stem cells and projection
775 neurons. Neuroscience *248*, 499–528

776 Dever, T.E., and Green, R. (2012). The elongation, termination, and recycling phases of
777 translation in eukaryotes. Cold Spring Harbor perspectives in biology *4*.

778 Ebert, B., and Lipton, J.M. (2011). Diamond Blackfan anemia and ribosome biogenesis:
779 introduction. Seminars in hematology *48*, 73-74.

780 Farkas, L.M., Haffner, C., Giger, T., Khaitovich, P., Nowick, K., Birchmeier, C., Pääbo, S., and
781 Huttner, W.B. (2008). Insulinoma-associated 1 has a panneurogenic role and promotes the
782 generation and expansion of basal progenitors in the developing mouse neocortex. Neuron *60*,
783 40-55.

784 Fujii, K., Shi, Z., Zhulyn, O., Denans, N., and Barna, M. (2017). Pervasive translational
785 regulation of the cell signalling circuitry underlies mammalian development. Nature
786 communications *8*, 14443.

787 Gabay, M., Li, Y., and Felsher, D.W. (2014). MYC activation is a hallmark of cancer initiation
788 and maintenance. Cold Spring Harbor perspectives in medicine *4*.

789 Gautier, E.-F.F., Ducamp, S., Leduc, M., Salnot, V., Guillonneau, F., Dussiot, M., Hale, J.,
790 Giarratana, M.-C.C., Raimbault, A., Douay, L.*, et al.* (2016). Comprehensive Proteomic Analysis
791 of Human Erythropoiesis. Cell reports *16*, 1470-1484.

792 Greene, N.D., and Copp, A.J. (2014). Neural tube defects. Annu Rev Neurosci *37*, 221-242.

793 Hart, J.R., Garner, A.L., Yu, J., Ito, Y., Sun, M., Ueno, L., Rhee, J.K., Baksh, M.M., Stefan, E.,
794 Hartl, M.*, et al.* (2014). Inhibitor of MYC identified in a Krohnke pyridine library. Proc Natl
795 Acad Sci U S A *111*, 12556-12561.

796 Hébert, J.M., and McConnell, S.K. (2000). Targeting of cre to the Foxg1 (BF-1) locus mediates
797 loxP recombination in the telencephalon and other developing head structures. Developmental
798 biology *222*, 296-306.

799 Hirsch, C.A., and Hiatt, H.H. (1966). Turnover of liver ribosomes in fed and in fasted rats. J.
800 Biol. Chem. *241*, 5936–5940.

801 Holmberg, J., and Perlmann, T. (2012). Maintaining differentiated cellular identity. Nat Rev
802 Genet *13*, 429-439.

803 Hrvatin, S., Deng, F., O'Donnell, C.W., Gifford, D.K., and Melton, D.A. (2014). MARIS:
804 method for analyzing RNA following intracellular sorting. PLoS One *9*, e89459.

805 Huang, D.W.a.W., Sherman, B.T., and Lempicki, R.A. (2009). Systematic and integrative
806 analysis of large gene lists using DAVID bioinformatics resources. Nature protocols *4*, 44-57.

807 Hunter, N.L., and Dymecki, S.M. (2007). Molecularly and temporally separable lineages form
808 the hindbrain roof plate and contribute differentially to the choroid plexus. Development
809 (Cambridge, England) *134*, 3449-3460.

810 Kerosuo, L., and Bronner, M.E. (2016). cMyc Regulates the Size of the Premigratory Neural
811 Crest Stem Cell Pool. Cell Rep *17*, 2648-2659.

812 Khajuria, R.K., Munschauer, M., Ulirsch, J.C., Fiorini, C., Ludwig, L.S., McFarland, S.K.,
813 Abdulhay, N.J., Specht, H., Keshishian, H., Mani, D.R.*, et al.* (2018). Ribosome Levels
814 Selectively Regulate Translation and Lineage Commitment in Human Hematopoiesis. Cell *173*,
815 90-103 e119.

816 Kondrashov, N., Pusic, A., Stumpf, C.R., Shimizu, K., Hsieh, A.C., Xue, S., Ishijima, J.,
817 Shiroishi, T., and Barna, M. (2011). Ribosome-mediated specificity in Hox mRNA translation
818 and vertebrate tissue patterning. Cell *145*, 383-397.

819 Kraushar, M.L., Popovitchenko, T., Volk, N.L., and Rasin, M.R. (2016). The frontier of RNA
820 metamorphosis and ribosome signature in neocortical development. International journal of
821 developmental neuroscience : the official journal of the International Society for Developmental
822 Neuroscience *55*, 131-139.

823 Kraushar, M.L., Thompson, K., Wijeratne, H.R., Viljetic, B., Sakers, K., Marson, J.W.,
824 Kontoyiannis, D.L., Buyske, S., Hart, R.P., and Rasin, M.R. (2014). Temporally defined
825 neocortical translation and polysome assembly are determined by the RNA-binding protein Hu
826 antigen R. Proceedings of the National Academy of Sciences of the United States of America
827 *111*, 24.

828 Kraushar, M.L., Viljetic, B., Wijeratne, H.R., Thompson, K., Jiao, X., Pike, J.W., Medvedeva,
829 V., Groszer, M., Kiledjian, M., Hart, R.P., et al. (2015). Thalamic WNT3 Secretion
830 Spatiotemporally Regulates the Neocortical Ribosome Signature and mRNA Translation to
831 Specify Neocortical Cell Subtypes. J. Neurosci. *35*, 10911–10926.

832 Kress, T.R., Sabò, A., and Amati, B. (2015). MYC: connecting selective transcriptional control
833 to global RNA production. Nature reviews Cancer *15*, 593-607.

834 Kwan, K.Y., Lam, M.M., Johnson, M.B., Dube, U., Shim, S., Rašin, M.-R.R., Sousa, A.M.M.M.,
835 Fertuzinhos, S., Chen, J.-G.G., Arellano, J.I.*, et al.* (2012). Species-dependent posttranscriptional
836 regulation of NOS1 by FMRP in the developing cerebral cortex. Cell *149*, 899-911.

837 Laplante, M., and Sabatini, D.M. (2012). mTOR signaling in growth control and disease. Cell
838 *149*, 274-293.

839 Lehtinen, M.K., Zappaterra, M.W., Chen, X., Yang, Y.J., Hill, A.D., Lun, M., Maynard, T.,
840 Gonzalez, D., Kim, S., Ye, P.*, et al.* (2011). The cerebrospinal fluid provides a proliferative
841 niche for neural progenitor cells. Neuron *69*, 893-905.

842 Lin, C.Y., Lovén, J., Rahl, P.B., Paranal, R.M., Burge, C.B., Bradner, J.E., Lee, T.I., and Young,
843 R.A. (2012). Transcriptional amplification in tumor cells with elevated c-Myc. Cell *151*, 56-67.

844 Liu, J., Xu, Y., Stoleru, D., and Salic, A. (2012). Imaging protein synthesis in cells and tissues
845 with an alkyne analog of puromycin. Proceedings of the National Academy of Sciences of the
846 United States of America *109*, 413-418.

847 Lun, M.P., Monuki, E.S., and Lehtinen, M.K. (2015). Development and functions of the choroid
848 plexus-cerebrospinal fluid system. Nature reviews Neuroscience *16*, 445-457.

849 Mahata, B., Sundqvist, A., and Xirodimas, D.P. (2012). Recruitment of RPL11 at promoter sites
850 of p53-regulated genes upon nucleolar stress through NEDD8 and in an Mdm2-dependent
851 manner. Oncogene *31*, 3060–3071.

852 Marzesco, A.-M.M., Janich, P., Wilsch-Bräuninger, M., Dubreuil, V., Langenfeld, K., Corbeil,
853 D., and Huttner, W.B. (2005). Release of extracellular membrane particles carrying the stem cell
854 marker prominin-1 (CD133) from neural progenitors and other epithelial cells. Journal of cell
855 science *118*, 2849-2858.

856 Massarwa, R., Ray, H.J., and Niswander, L. (2014). Morphogenetic movements in the neural
857 plate and neural tube: mouse. Wiley Interdiscip Rev Dev Biol *3*, 59-68.

858 Massarwa, R.a., and Niswander, L. (2013). In toto live imaging of mouse morphogenesis and
859 new insights into neural tube closure. Development (Cambridge, England) *140*, 226-236.

860 Momota, H., Shih, A.H., Edgar, M.A., and Holland, E.C. (2008). c-Myc and beta-catenin
861 cooperate with loss of p53 to generate multiple members of the primitive neuroectodermal tumor
862 family in mice. Oncogene *27*, 4392-4401.

863 Monuki, E.S. (2007). The morphogen signaling network in forebrain development and
864 holoprosencephaly. Journal of neuropathology and experimental neurology *66*, 566-575.

865 Nie, Z., Hu, G., Wei, G., Cui, K., Yamane, A., Resch, W., Wang, R., Green, D.R., Tessarollo, L.,
866 Casellas, R.*, et al.* (2012). c-Myc is a universal amplifier of expressed genes in lymphocytes and
867 embryonic stem cells. Cell *151*, 68-79.

868 Nikolov, E.N., Dabeva, M.D., and Nikolov, T.K. (1983). Turnover of ribosomes in regenerating
869 rat liver. Int. J. Biochem. *15*, 1255–1260.

870 Pilaz, L.J., Lennox, A.L., Rouanet, J.P., and Silver, D.L. (2016). Dynamic mRNA Transport and
871 Local Translation in Radial Glial Progenitors of the Developing Brain. Current biology : CB *26*,
872 3383-3392.

873 Pilaz, L.J., and Silver, D.L. (2017). Moving messages in the developing brain-emerging roles for
874 mRNA transport and local translation in neural stem cells. FEBS letters.

875 Poduri, A., Evrony, G.D., Cai, X., Elhosary, P.C., Beroukhim, R., Lehtinen, M.K., Hills, L.B.,
876 Heinzen, E.L., Hill, A., Hill, R.S.*, et al.* (2012). Somatic activation of AKT3 causes hemispheric
877 developmental brain malformations. Neuron *74*, 41-48.

878 Popovitchenko, T., Thompson, K., Viljetic, B., Jiao, X., Kontonyiannis, D.L., Kiledjian, M.,
879 Hart, R.P., and Rasin, M.R. (2016). The RNA binding protein HuR determines the differential
880 translation of autism-associated FoxP subfamily members in the developing neocortex. Scientific
881 reports *6*, 28998.

882 Rallu, M., Corbin, J.G., and Fishell, G. (2002). Parsing the prosencephalon. Nature reviews
883 Neuroscience *3*, 943-951.

884 Rasin, M.R., and Silver, D. (2016). The crossroads of RNA regulation and function in
885 neurodevelopment. Int J Dev Neurosci *55*, 101.

886 Sanchez, C.G., Teixeira, F.K., Czech, B., Preall, J.B., Zamparini, A.L., Seifert, J.R., Malone,
887 C.D., Hannon, G.J., and Lehmann, R. (2016). Regulation of Ribosome Biogenesis and Protein
888 Synthesis Controls Germline Stem Cell Differentiation. Cell stem cell *18*, 276-290.

889 Scognamiglio, R., Cabezas-Wallscheid, N., Thier, M., Altamura, S., Reyes, A., Prendergast,
890 Á.M., Baumgärtner, D., Carnevalli, L.S., Atzberger, A., Haas, S.*, et al.* (2016). Myc Depletion
891 Induces a Pluripotent Dormant State Mimicking Diapause. Cell *164*, 668-680.

892 Shannon, M.L., Fame, R.M., Chau, K.F., Dani, N., Calicchio, M.L., Geleoc, G.S., Lidov,
893 H.G.W., Alexandrescu, S., and Lehtinen, M.K. (2018). Mice Expressing c-MYC in Neural
894 Precursors Develop Choroid Plexus and Ciliary Body Tumors. Am J Pathol. *Epub ahead of*
895 *print.*

896 Shi, Z., and Barna, M. (2015). Translating the genome in time and space: specialized ribosomes,
897 RNA regulons, and RNA-binding proteins. Annual review of cell and developmental biology *31*,
898 31-54.

899 Shi, Z., Fujii, K., Kovary, K.M., Genuth, N.R., Rost, H.L., Teruel, M.N., and Barna, M. (2017).
900 Heterogeneous Ribosomes Preferentially Translate Distinct Subpools of mRNAs Genome-wide.
901 Mol Cell *67*, 71-83 e77.

902 Silvera, D., Formenti, S.C., and Schneider, R.J. (2010). Translational control in cancer. Nature
903 reviews Cancer *10*, 254-266.

904 Simsek, D., Tiu, G.C., Flynn, R.A., Byeon, G.W., Leppek, K., Xu, A.F., Chang, H.Y., and
905 Barna, M. (2017). The Mammalian Ribo-interactome Reveals Ribosome Functional Diversity
906 and Heterogeneity. Cell *169*, 1051-1594097664.

907 Subramanian, A., Tamayo, P., Mootha, V.K., Mukherjee, S., Ebert, B.L., Gillette, M.A.,
908 Paulovich, A., Pomeroy, S.L., Golub, T.R., Lander, E.S.*, et al.* (2005). Gene set enrichment
909 analysis: A knowledge-based approach for interpreting genome-wide expression profiles.
910 Proceedings of the National Academy of Sciences of the United States of America *102*, 15545-
911 15550.

912 Sur, M., and Rubenstein, J.L. (2005). Patterning and plasticity of the cerebral cortex. Science
913 (New York, NY) *310*, 805-810.

914 Tavano, S., Taverna, E., Kalebic, N., Haffner, C., Namba, T., Dahl, A., Wilsch-Brauninger, M.,
915 Paridaen, J., and Huttner, W.B. (2018). Insm1 Induces Neural Progenitor Delamination in
916 Developing Neocortex via Downregulation of the Adherens Junction Belt-Specific Protein
917 Plekha7. Neuron *97*, 1299-1314 e1298.

Tiku, V., Jain, C., Raz, Y., Nakamura, S., Heestand, B., Liu, W., Spath, M., Suchiman, H.E.D., Muller, R.U., Slagboom, P.E.*, et al.* (2016). Small nucleoli are a cellular hallmark of longevity. Nat Commun *8*, 16083.

Topol, A., English, J.A., Flaherty, E., Rajarajan, P., Hartley, B.J., Gupta, S., Desland, F., Zhu, S., Goff, T., Friedman, L.*, et al.* (2015). Increased abundance of translation machinery in stem cell-derived neural progenitor cells from four schizophrenia patients. Transl Psychiatry *5*, e662.

Toyoda, R., Assimacopoulos, S., Wilcoxon, J., Taylor, A., Feldman, P., Suzuki-Hirano, A., Shimogori, T., and Grove, E.A. (2010). FGF8 acts as a classic diffusible morphogen to pattern the neocortex. Development (Cambridge, England) *137*, 3439-3448.

Trapnell, C., Roberts, A., Goff, L., Pertea, G., Kim, D., Kelley, D.R., Pimentel, H., Salzberg, S.L., Rinn, J.L., and Pachter, L. (2012). Differential gene and transcript expression analysis of RNA-seq experiments with TopHat and Cufflinks. Nature protocols *7*, 562-578.

Tronche, F., Kellendonk, C., Kretz, O., Gass, P., Anlag, K., Orban, P.C., Bock, R., Klein, R., and Schütz, G. (1999). Disruption of the glucocorticoid receptor gene in the nervous system results in reduced anxiety. Nature genetics *23*, 99-103.

van Riggelen, J., Yetil, A., and Felsher, D.W. (2010). MYC as a regulator of ribosome biogenesis and protein synthesis. Nature reviews Cancer *10*, 301-309.

Wallingford, J.B., Niswander, L.A., Shaw, G.M., and Finnell, R.H. (2013). The continuing challenge of understanding, preventing, and treating neural tube defects. Science (New York, NY) *339*, 1222002.

Warner, J.R., and McIntosh, K.B. (2009). How common are extraribosomal functions of ribosomal proteins? Mol. Cell *34*, 3–11.

Wilde, J.J., Petersen, J.R., and Niswander, L. (2014). Genetic, epigenetic, and environmental contributions to neural tube closure. Annual review of genetics *48*, 583-611.

Yu, J., Baybis, M., Lee, A., McKhann, G., 2nd, Chugani, D., Kupsky, W.J., Aronica, E., and Crino, P.B. (2005). Targeted gene expression analysis in hemimegalencephaly: activation of beta-catenin signaling. Brain Pathol *15*, 179-186.

Zeller, K.I., Jegga, A.G., Aronow, B.J., O'Donnell, K.A., and Dang, C.V. (2003). An integrated database of genes responsive to the Myc oncogenic transcription factor: identification of direct genomic targets. Genome biology *4*.

Zhou, X., Liao, W.-J.J., Liao, J.-M.M., Liao, P., and Lu, H. (2015). Ribosomal proteins: functions beyond the ribosome. J Mol Cell Biol *7*, 92–104.

Zinin, N., Adameyko, I., Wilhelm, M., Fritz, N., Uhlen, P., Ernfors, P., and Henriksson, M.A. (2014). MYC proteins promote neuronal differentiation by controlling the mode of progenitor cell division. EMBO Rep *15*, 383-391.

FIGURE LEGENDS

Figure 1. Transcriptome analysis of microdissected forebrain epithelium reveals downregulation of genes encoding protein biosynthetic machinery. (A) Schematic of E8.5 embryo with open forebrain neural tube (left) and E10.5 embryo (right). Shaded regions encircled by dotted line denote developing forebrain epithelium microdissected for RNAseq. **(B)** Heatmap and hierarchical clustering of ~3,900 differentially expressed genes ($q < 0.05$): 2,375 genes were enriched in E8.5 and 1,523 genes were enriched in E10.5. Each biological replicate contained tissue pooled from one litter of embryos. Red and green indicate relatively higher and lower expression, with gene FPKM values log2 transformed, centered and scaled by rows for display purposes. **(C, D)** MA plot displaying genes encoding secreted factors (C), and receptors (D). Each dot represents a single gene. Red dots denote differentially expressed genes as identified by Cuffdiff. Genes below blue line (y=0) are enriched in E8.5. **(E)** Functional annotation clustering of E8.5 neuroepithelium enriched genes revealed overrepresentation of genes encoding ribosomal proteins, ribosome biogenesis and translation factors. The top five enriched functional clusters are shown. **(F)** Functional annotation clustering of E10.5 neuroepithelium enriched genes shows overrepresentation of genes needed for neuron differentiation. The top five enriched functional clusters are shown. **(G-I)** GSEA of E8.5 versus E10.5 neuroepithelium for gene sets involved in ribosome biogenesis and translation. Broad Institute Molecular Signatures Database Identifiers: KEGG_RIBOSOME (G), GO_RIBOSOME_BIOGENESIS (H), and TRANSLATION (I). Each line represents a single gene in the gene set. Genes on the right side are enriched in E8.5. **(J-L)** Correlation plots of average expression (log2 transformed FPKM) at E8.5 and E10.5 for ribosomal proteins (J), translation factors (K), and all differentially expressed genes (L). In all cases correlation was

982 significant; ribosomal proteins (J), Spearman R=0.91, p<0.0001; translation factors (K)
983 Spearman R=0.98, p<0.0001; and DEG (L), Spearman R=0.82, p<0.0001.
984
985 **Figure 1-figure supplement 1. Differential gene expression between E8.5 and E10.5**
986 **neuroepithelium.** (**A**) MA plot displaying all expressed genes (FPKM > 1) in E8.5 and E10.5
987 neuroepithelium. Red dots denote differentially expressed genes identified by Cuffdiff. Genes
988 below blue line (y=0) are enriched in E8.5. (**B**) Quantitative RT-PCR (qRT-PCR) validation of
989 75 genes showed positive correlation (R^2=0.58) with RNAseq data. (**C**) RNAseq showed
990 upregulation of glial markers, *Glast* (left) and *Blbp* (right), in E10.5 neuroepithelium; y-axis
991 shows FPKM values.
992
993 **Figure 2. Ribosome biogenesis decreases from E8.5 to E10.5. (A, B)** MA plot displaying
994 genes encoding ribosomal proteins (A), ribosome biogenesis factors (B). Each dot represents a
995 single gene. Red dots denote differentially expressed genes as identified by Cuffdiff. Genes
996 below blue line (y=0) are enriched in E8.5. **(C)** Immunohistochemistry of the nucleolar protein
997 Fibrillarin (green) in E8.5, E10.5 and E14.5 neuroepithelium. Scale bar = 20 μm. **(D)** Example of
998 z-stack image of Fibrillarin staining (left) and 3D reconstruction of nucleoli using Imaris (right).
999 **(E)** Quantification of nucleolar volume using Imaris. Each data point represents one nucleolus.
1000 *p≤0.05, **p≤0.01, Welch's ANOVA with Games-Howell post-hoc test. Sample size, E8.5:
1001 n=135 from 3 embryos; E10.5: n=139 from 3 embryos; E14.5: n=146 from 3 embryos. **(F, G)**
1002 Representative images of fluorescent in situ hybridization of 5.8S pre-rRNA (red, F) and 5.8S
1003 total rRNA (green, G). **(H)** Y10b immunostaining shows higher levels of 5.8S rRNA in E8.5
1004 than E10.5 neuroepithelium. Scale bar = 20 μm. **(I)** Quantification of 5.8S pre-rRNA signal

shows larger nucleolar area in E8.5 compared to E10.5 neuroepithelium. Each data point represents one nucleolus. ****p≤0.0001, Welch's t-test. Sample size, E8.5: n= 150 from 3 embryos; E10.5: n = 202 from 3 embryos. **(J)** Average nucleolar area in E8.5 vs. E10.5 embryo. **p≤0.01, unpaired t-test, n = 3 embryos. **(K, L)** RPL11 (K, red) and RPS12 (L, red) were more highly expressed along the apical surface of E8.5 than E10.5 neuroepithelium. Phospho-Vimentin (P-Vim, green) labels dividing progenitors. Scale bar = 20 μm. **(M)** Immuoblotting shows similar expression of RPL10A between E8.5 and E10.5. **(N)** Representative images of TEM in neuroepithelial cells at E8.5 and R10.5. **(O-Q)** Quantification of TEM ribosomal number per standardized field of view, 78,736 nm^2, (O), ribosomal density in cytoplasm (P), and percent of the standard field of view occupied by membrane-bound organelles (Q). *p≤0.05, **p≤0.01, Unpaired t-test.

Figure 3. Down-regulation of mTOR signaling pathway and decreased protein synthesis in E10.5 forebrain progenitors. **(A)** MA plot displaying genes encoding translation factors. Each dot represents a single gene. Red dots denote differentially expressed genes as identified by Cuffdiff. Genes below blue line (y=0) are enriched in E8.5. **(B)** Immunostaining of developing forebrain progenitors shows higher expression of the translation initiation factor EIF3η (green) in E8.5 versus E10.5 neuroepithelium. Scale bar = 20 μm. **(C)** Immunostaining of developing forebrain neuroepithelium shows decreased phosphorylation of 4E-BP1 (red) in E10.5 neuroepithelium. Scale bar 20 μm. **(D)** Immunoblotting shows decreased expression and phosphorylation of 4E-BP1 at E10.5. **(E)** Immunoblotting shows decreased phosphorylation of S6K at E10.5. **(F)** Immunostaining of developing forebrain neuroepithelium shows decreased

phosphorylation of ribosomal protein S6 (red) in E10.5 neuroepithelium. Scale bar 20 μm. **(G)** Immunoblotting shows decreased phosphorylation of ribosomal protein S6 at E10.5. **(H)** Schematic of OPP injection into pregnant dams and incorporation into translating polypeptides in the embryos. **(I)** OPP incorporation assay in E8.5 and E10.5 developing forebrain neuroepithelium. **(J)** Quantification of OPP fluorescence intensity using Image J shows decreased rate of protein synthesis at E10.5. **$p \leq 0.01$ Welch's t-test. For each age, n=9 embryos from 3 litters.

Figure 4. Downregulation of protein biosynthetic machinery during early forebrain development matches the AF and CSF proteomes. (A) Plot showing all proteins/genes that are detected in both AF/CSF and the neighboring neuroepithelium. Each dot represents a single protein/gene. Red dots denote differentially expressed genes between E8.5 and E10.5 epithelium. Genes left of x=0 were enriched in E8.5 epithelium whereas proteins below y=0 were enriched in E8.5 AF. Therefore, genes/proteins in lower left quadrant (shaded) were enriched in both E8.5 epithelium and AF. MS = mass spectrometry. **(B)** Functional annotation clustering of genes/proteins enriched in both E8.5 epithelium and AF (genes/proteins in shaded quadrant in (A)) shows that ribosomes/translation is the most overrepresented category. **(C, D)** Comparison of AF/CSF proteomes with neuroepithelium transcriptome showed that most ribosomal proteins and translation factors enriched in E8.5 AF were enriched in age-matched epithelium (shaded quadrants). **(E)** Schematics depicting the specific ribosomal protein subunits that were detected in E8.5 AF (left) and E10.5 CSF (right). Subunits with blue and orange were detected in both fluid and tissue, whereas those in orange were only detected in tissue.

Figure 5. MYC modulates ribosome biogenesis in the developing forebrain. (A) MA plot displaying genes encoding transcription factors in E8.5 and E10.5 neuroepithelium. Each dot represents a single gene. Red dots denote differentially expressed genes identified by Cuffdiff. Genes below blue line (y=0) enriched in E8.5. *Myc* (arrow) expression is ~10 fold higher in E8.5 epithelium (FPKM: E8.5 = 28.73, E10.5 = 2.76). **(B)** MYC expression was enriched in E8.5 neuroepithelium. Once downregulated at E10.5, MYC expression remained low throughout cortical development. Scale bar = 20 μm. **(C, D)** GSEA of E8.5 versus E10.5 neuroepithelium for gene sets containing genes up-regulated by MYC and whose promoters are bound by MYC (C), and E-box containing MYC target genes (D). Broad Institute Molecular Signatures Database Identifiers: DANG_MYC_TARGETS_UP (C), BENPORATH_MYC_TARGETS_WITH _EBOX (D). Each line represents a single gene in the gene set; genes on the right side enriched in E8.5. **(E)** Quantification of nucleolar volume of E8.5 embryos treated with vehicle control or KJ-Pyr-9 for 24 hours. Each data point represents one nucleolus. ***$p \leq 0.001$, Welch's t-test. Sample size, vehicle: n=140 from 3 embryos; KJ-Pyr-9: n=140 from 3 embryos. **(F)** Quantification of nucleolar volume of $Myc^{-/-}$ compared to controls (wild type and heterozygous littermates) in E8.5 neuroepithelium. *$p \leq 0.05$ Unpaired t-test. Sample size, controls: n=238 from 5 embryos; $Myc^{-/-}$: n=97 from 2 embryos. **(G)** Immunostaining shows overexpression of MYC (red) in the developing cortex of E12.5 MYC-OE (right) embryos from the *Nestin-cre* x StopFLMYC cross. TUJ1 (green) staining labels neurons. **(H)** Functional annotation clustering of the 105 MYC-OE enriched genes shows overrepresentation of genes encoding ribosome constituents. The top five enriched functional clusters are shown. **(I, J)** GSEA of WT versus MYC-OE apical progenitors for gene sets involved in ribosome biogenesis. Broad Institute Molecular Signatures Database Identifiers: KEGG_RIBOSOME (I), and GO_RIBOSOME_

BIOGENESIS (J). Each line represents a single gene in the gene set, genes on the right side are enriched in MYC-OE. **(K)** Heatmap of the 43 ribosomal protein genes that are differentially expressed between MYC-OE and WT apical progenitors (* q<0.3, **q<0.1). All ribosomal proteins are more highly expressed in MYC-OE. Red and green indicate relatively higher and lower expression, with gene FPKM values log2 transformed. **(L)** MA plot displaying genes encoding ribosomal proteins in E13.5 apical progenitors. Each dot represents a single gene. Red dots denote differentially expressed genes as identified by Cuffdiff. Genes above blue line (y=0) are enriched in MYC-OE. **(M)** Quantification of nucleolar volume of WT and MYC-OE (*Foxg1-cre* driven) forebrain progenitors at E11.5. Each data point represents one nucleolus. ****p≤0.0001, Welch's t-test. Sample size, WT: n=194 from 4 embryos; MYC-OE: n=144 from 3 embryos. **(N)** Quantification of nucleolar volume of WT and MYC-OE (*Nestin-cre* driven) apical progenitors at E13.5. Each data point represents one nucleolus. ***p≤0.001, Welch's t-test. Sample size, WT: n=234 from 5 embryos; MYC-OE: n=248 from 5 embryos.

Figure 5-figure supplement 1. MYC expression and mouse models. (A) Quantitative RT-PCR validated higher expression of *Myc* in the developing neuroepithelium of E8.5. *P<0.05, Welch's t-test. Each data point represents multiple embryos from the same litter. **(B)** Immunoblotting shows higher expression of MYC in E8.5 developing forebrain. See also (Shannon et al., 2018). **(C)** Immunostaining confirmed specificity of MYC antibody. **(D)** Representative E9.5 wildtype embryo (left) and *Myc*-deficient littermates ($Myc^{-/-}$, right panels), which show range of phenotypes (Davis et al., 1993) including small size ($Myc^{+/+}$: 0%, 0/17; $Myc^{+/-}$: 20%, 5/25; $Myc^{-/-}$: 67%, 6/9), incomplete neural tube closure ($Myc^{+/+}$: 0%, 0/17; $Myc^{+/-}$: 0%, 0/25; $Myc^{-/-}$: 11%, 1/9), and delayed development ($Myc^{+/+}$: 12%, 2/17; $Myc^{+/-}$: 4%, 1/25; $Myc^{-/-}$: 22%, 2/9).

Morphologically the representative *Myc*$^{-/-}$ embryos are similar to a normal E8.25 before turning, and have open neural tubes. Scale bar = 0.5mm. **(E)** Quantitative RT-PCR confirms higher expression of *Myc* in E12.5 neuroepithelium of MYC-OE embryos than in wildtype littermates from the *Nestin-cre* x StopFLMYC cross. **≤0.01, Welch's t-test, n=5 (WT) or 6 (MYC-OE) embryos from 2 litters. **(F)** Immunoblotting confirms overexpression of MYC (top) in the developing forebrain of E12.5 MYC-OE from the *Nestin-cre* x StopFLMYC cross. Bottom panel shows ACTB loading control. **(G)** Immunostaining shows overexpression of MYC (red) in the developing cortex of E10.5 MYC-OE (right) embryos from the *Foxg1-cre* x StopFLMYC cross. Scale bar = 20 μm. **(H)** Representative FACS profile used for isolating apical progenitors form E13.5 cortex. Apical progenitors (PAX6-high, TUJ1-low) are selected using the lower right gate. Upper left gate represents neurons (PAX6-low, TUJ1-high). **(I)** Heatmap and hierarchical clustering of the 135 genes that are differentially expressed between MYC-OE and WT apical progenitors ($q < 0.1$). 105 genes are enriched in MYC-OE (*Nestin-cre* driven), whereas 30 genes are repressed. Each biological replicate contains cells from 2 – 4 embryos. Red and green indicate relatively higher and lower expression, with gene FPKM values log2 transformed, and centered and scaled by rows for display purposes. **(J, K)** GSEA of WT versus MYC-OE apical progenitors for gene sets containing genes upregulated by MYC and whose promoters are bound by MYC. Broad Institute Molecular Signatures Database Identifiers: DANG_MYC_TARGETS_UP (J) and TRANSLATION (K).

Figure 6. Persistent MYC expression in cortical progenitors leads to macrocephaly. (A) Representative images of E14.5 brains from WT and MYC-OE from the *Nestin-cre* x StopFLMYC cross. Scale bar = 2mm. **(B)** Quantification of E14.5 cortical length (olfactory bulb

excluded). *p≤0.05, unpaired t-test, WT: n=6 from 2 litters, MYC-OE: n=10 embryos from 2 litters. **(C)** Quantification of E14.5 cortical area. Cortical area of one hemisphere was measured (olfactory bulb excluded). p>0.05, unpaired t-test, WT: n=6 from 2 litters, MYC-OE: n=10 embryos from 2 litters. **(D)** Representative images of P0 brains from WT and MYC-OE from the *Nestin-cre* x StopFLMYC cross. Scale bar = 2mm. **(E)** Quantification of P0 brain weight. Olfactory bulb, medulla and pons were excluded from measurements. ****p≤0.0001, unpaired t-test, No outliers, WT: n=10 pups from 3 litters, MYC-OE: n=12 pups from 3 litters. **(F)** Quantification of P0 cortical length as in (B). ****p≤0.0001, unpaired t-test, outlier excluded by ROUT method, WT: n=10 pups from 3 litters, MYC-OE: n=11 pups from 3 litters. **(G)** Quantification of P0 cortical area as in (C). ****p≤0.0001, Welch's t-test, outlier excluded by ROUT method, WT: n=10 pups from 3 litters, MYC-OE: n=11 pups from 3 litters. **(H)** Percent PAX6-positive progenitors that were also BrdU-positive after a 2 hour BrdU pulse at E15.5. *p≤0.05, Welch's t-test, n=5 embryos from 3 litters. **(I)** Representative H&E staining of WT and MYC-OE forebrain at P0. **(J)** Quantification of cortical thickness of P0 cortex. Thickness is measured from the ventricular surface to the pial surface in the dorsal-lateral cortex. p>0.05, unpaired t-test, n=6 pups from 5 litters. **(K)** MYC-OE had increased number of CUX1-positive upper layer neurons at P0. **p≤0.01; paired t-test, n=4 litters, 1-2 pairs of embryos per litter were quantified. **(L)** Examples of 100μm wide cortical columns at P0 used for cell counting. CUX1: upper layer neurons (red), CTIP2: lower layer neurons (green).

Figure 6-figure supplement 1. MYC overexpression in neural progenitors driven by *Foxg1-cre* leads to slightly longer cortex at E14.5. **(A)** Quantitative RT-PCR validated higher expression of *Igf2* in the developing cortex of MYC-OE embryos. *P<0.05, unpaired t-test. n=6

embryos from 2 litters. **(B)** Representative images showing wildtype (left) and MYC-OE (right) brains at E14.5**.** Scale bar = 2 mm. **(C)** Quantification of E14.5 cortical length. The olfactory bulb was excluded from measurements. **p≤0.01, Welch's t-test, WT: 15 embryos from 6 litters; MYC-OE: 12 embryos from 6 litters. **(D)** Quantification of E14.5 cortical area. Cortical area of one hemisphere was measured (olfactory bulb excluded). P>0.05, unpaired t-test, WT: 15 embryos from 6 litters; MYC-OE: 12 embryos from 6 litters. ns = not significant.

Supplementary File 1. E8.5 vs E10.5 neuroepithelium RNA sequencing data: All genes (sheet 1), differentially expressed genes (DEG, sheet 2), DAVID functional annotation clustering (FAC, sheet 3 and 4), gene lists used for MA plot (sheet 5 – 10).

Supplementary File 2. WT vs MYC-OE apical progenitors RNA sequencing data: All genes (sheet 1), DEG (sheet 2), FAC of MYC-OE enriched genes (sheet 3), ribosomal protein genes used for MA plot in Figure 5L.

Figure 1

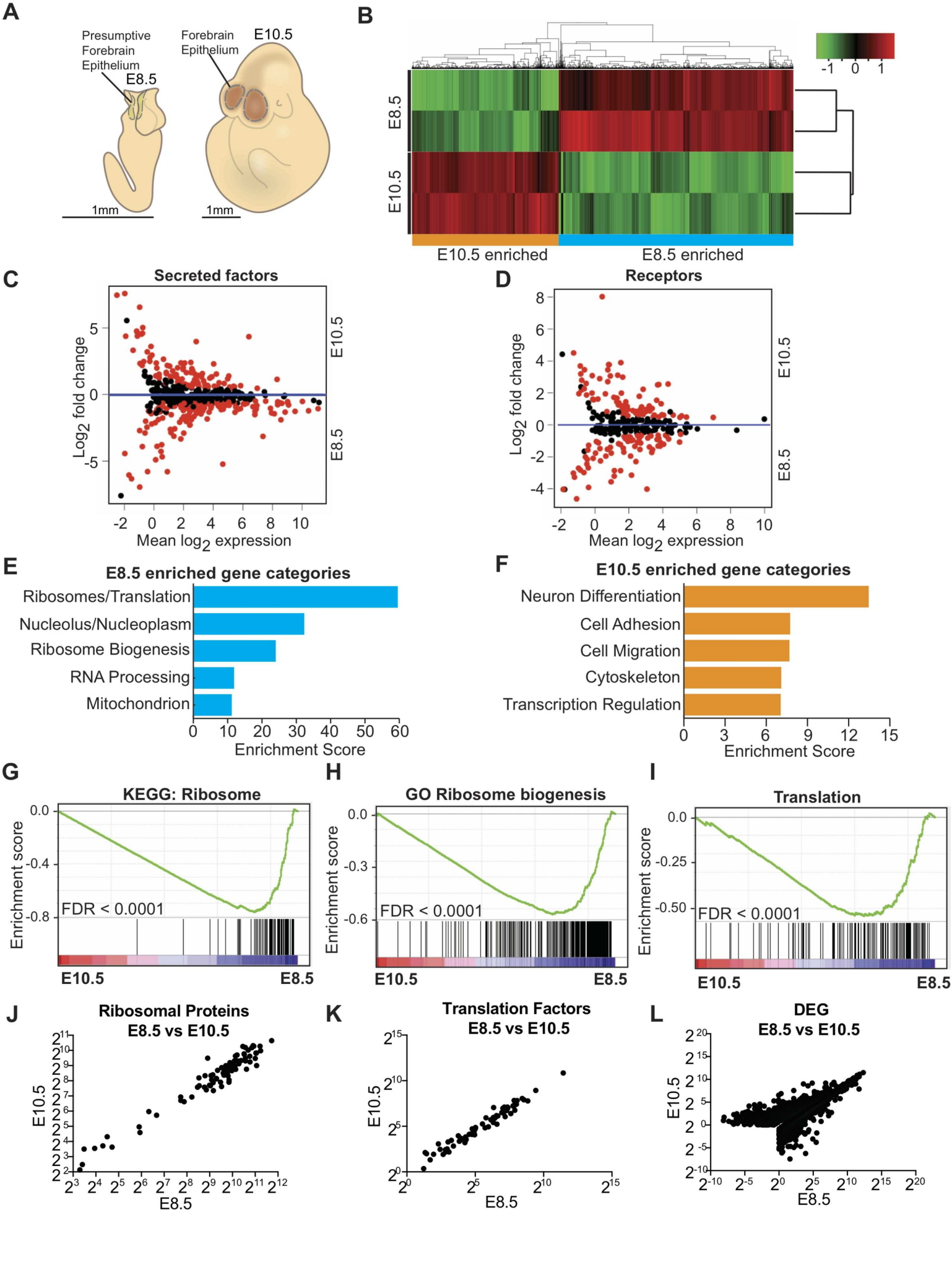
A
Presumptive Forebrain Epithelium
E8.5
Forebrain Epithelium
E10.5
1mm
1mm
B
E8.5
E10.5
-1 0 1
E10.5 enriched
E8.5 enriched
C
Secreted factors
Log2 fold change
E10.5
E8.5
Mean log2 expression
D
Receptors
Log2 fold change
E10.5
E8.5
Mean log2 expression
E
E8.5 enriched gene categories
Ribosomes/Translation
Nucleolus/Nucleoplasm
Ribosome Biogenesis
RNA Processing
Mitochondrion
Enrichment Score
F
E10.5 enriched gene categories
Neuron Differentiation
Cell Adhesion
Cell Migration
Cytoskeleton
Transcription Regulation
Enrichment Score
G
KEGG: Ribosome
Enrichment score
FDR < 0.0001
E10.5
E8.5
H
GO Ribosome biogenesis
Enrichment score
FDR < 0.0001
E10.5
E8.5
I
Translation
Enrichment score
FDR < 0.0001
E10.5
E8.5
J
Ribosomal Proteins
E8.5 vs E10.5
E10.5
E8.5
K
Translation Factors
E8.5 vs E10.5
E10.5
E8.5
L
DEG
E8.5 vs E10.5
E10.5
E8.5

Figure 2

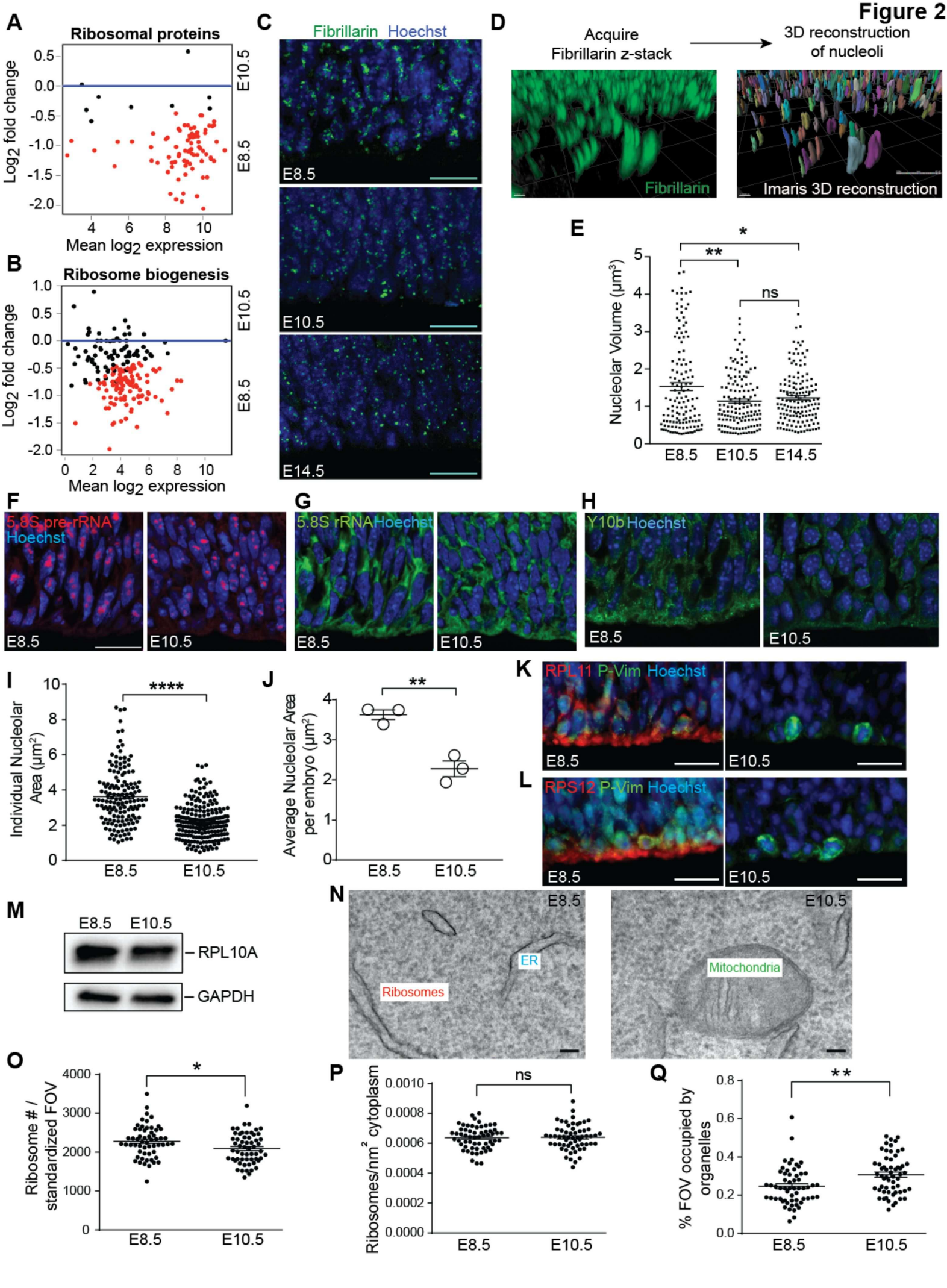
A
Ribosomal proteins
Log2 fold change
Mean log2 expression
E10.5
E8.5
B
Ribosome biogenesis
C
Fibrillarin Hoechst
E8.5
E10.5
E14.5
D
Acquire
Fibrillarin z-stack
3D reconstruction
of nucleoli
Fibrillarin
Imaris 3D reconstruction
E
Nucleolar Volume (µm³)
*
**
ns
E8.5
E10.5
E14.5
F
5.8S pre-rRNA
Hoechst
G
5.8S rRNA Hoechst
H
Y10b Hoechst
I
Individual Nucleolar Area (µm²)
****
J
Average Nucleolar Area per embryo (µm²)
**
K
RPL11 P-Vim Hoechst
L
RPS12 P-Vim Hoechst
M
RPL10A
GAPDH
N
ER
Ribosomes
Mitochondria
O
Ribosome # / standardized FOV
P
Ribosomes/nm² cytoplasm
Q
% FOV occupied by organelles

Figure 3

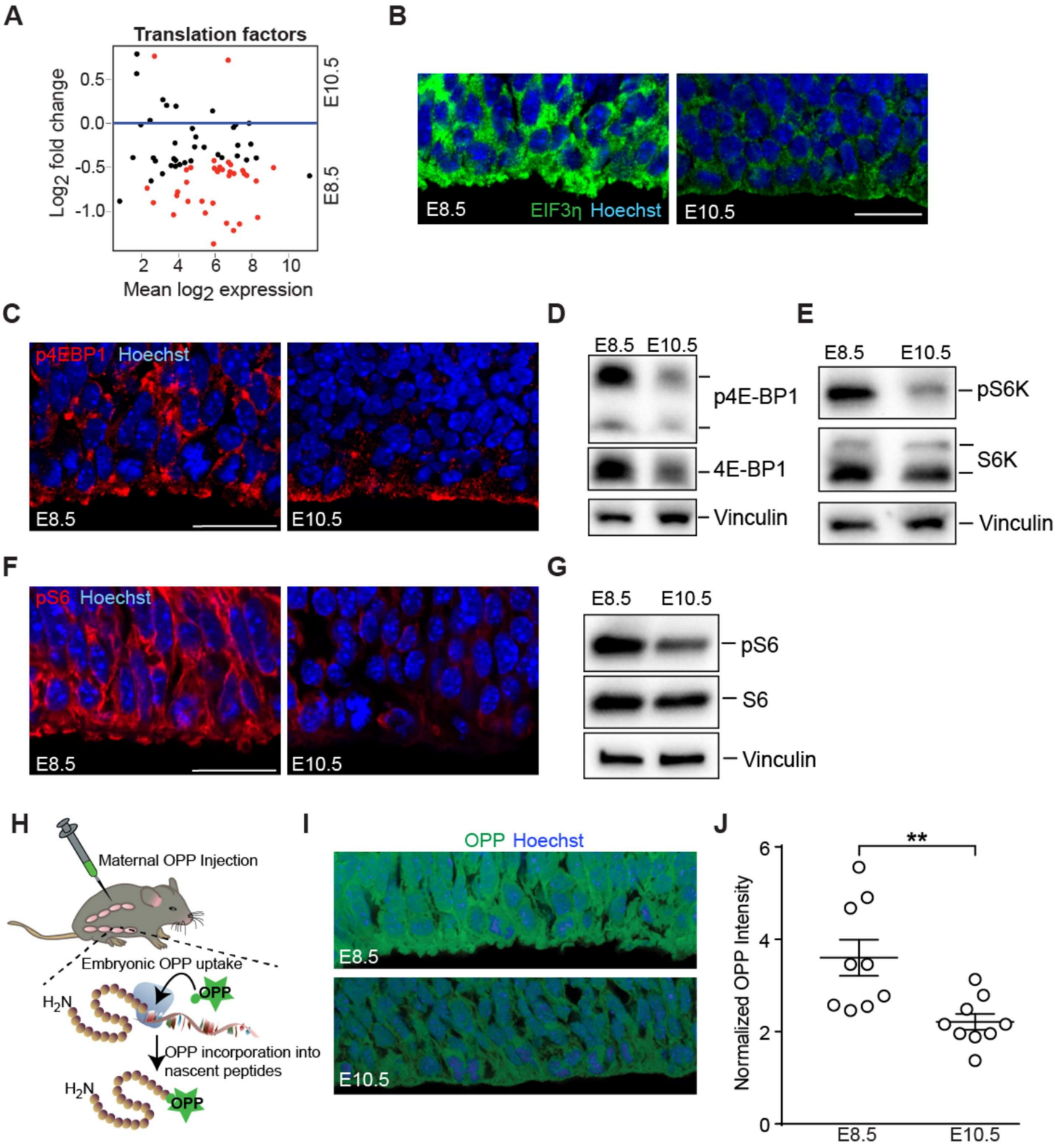
A
Translation factors
Log2 fold change
0.5
0.0
-0.5
-1.0
E10.5
E8.5
2
4
6
8
10
Mean log2 expression
B
E8.5
EIF3η Hoechst
E10.5
C
p4EBP1 Hoechst
E8.5
E10.5
D
E8.5 E10.5
p4E-BP1
4E-BP1
Vinculin
E
E8.5 E10.5
pS6K
S6K
Vinculin
F
pS6 Hoechst
E8.5
E10.5
G
E8.5 E10.5
pS6
S6
Vinculin
H
Maternal OPP Injection
Embryonic OPP uptake
H2N
OPP
OPP incorporation into nascent peptides
H2N
OPP
I
OPP Hoechst
E8.5
E10.5
J
**
Normalized OPP Intensity
6
4
2
0
E8.5
E10.5

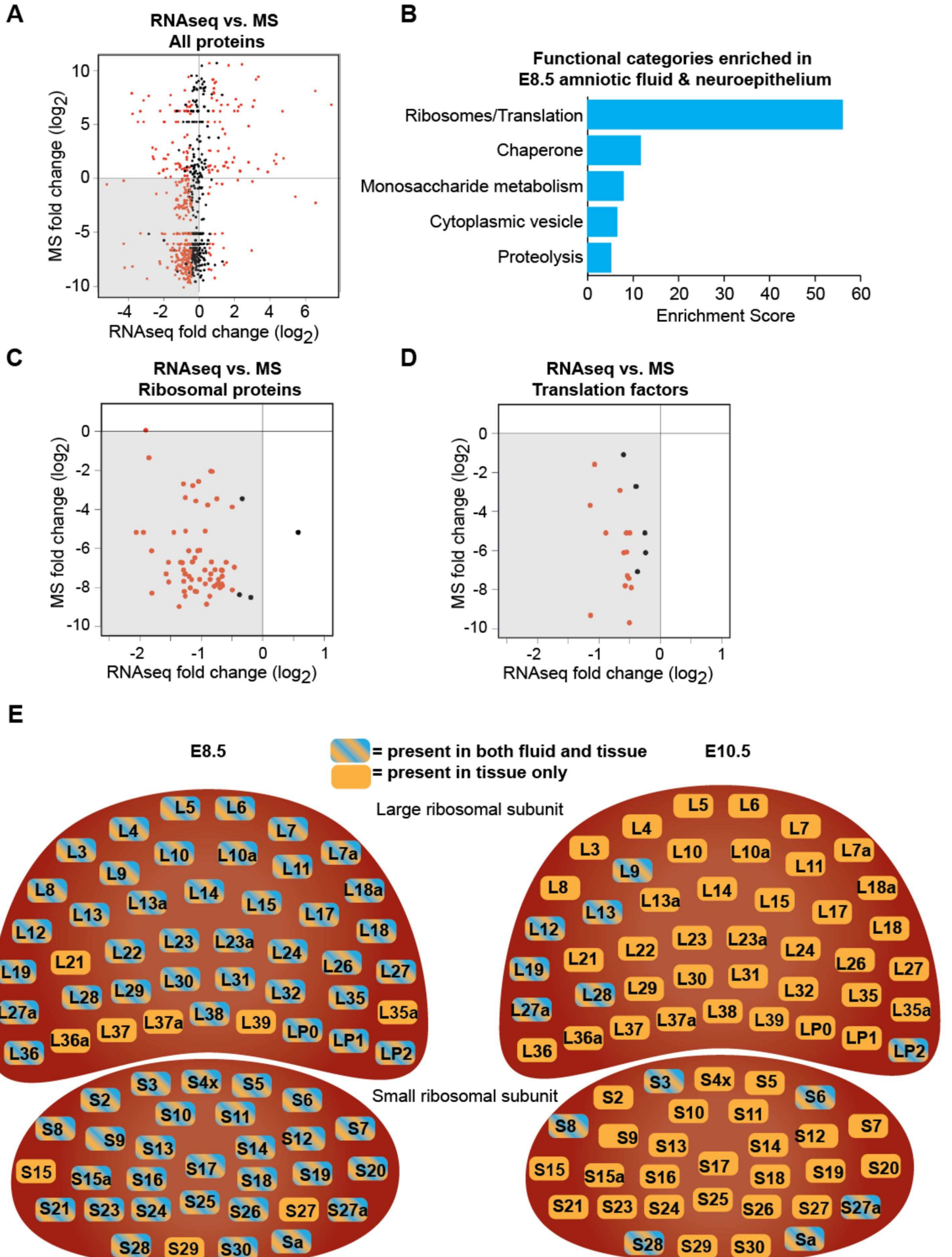
A
RNAseq vs. MS
All proteins
MS fold change (log2)
RNAseq fold change (log2)
B
Functional categories enriched in
E8.5 amniotic fluid & neuroepithelium
Ribosomes/Translation
Chaperone
Monosaccharide metabolism
Cytoplasmic vesicle
Proteolysis
Enrichment Score
C
RNAseq vs. MS
Ribosomal proteins
D
RNAseq vs. MS
Translation factors
E
E8.5
= present in both fluid and tissue
= present in tissue only
E10.5
Large ribosomal subunit
Small ribosomal subunit

Figure 5

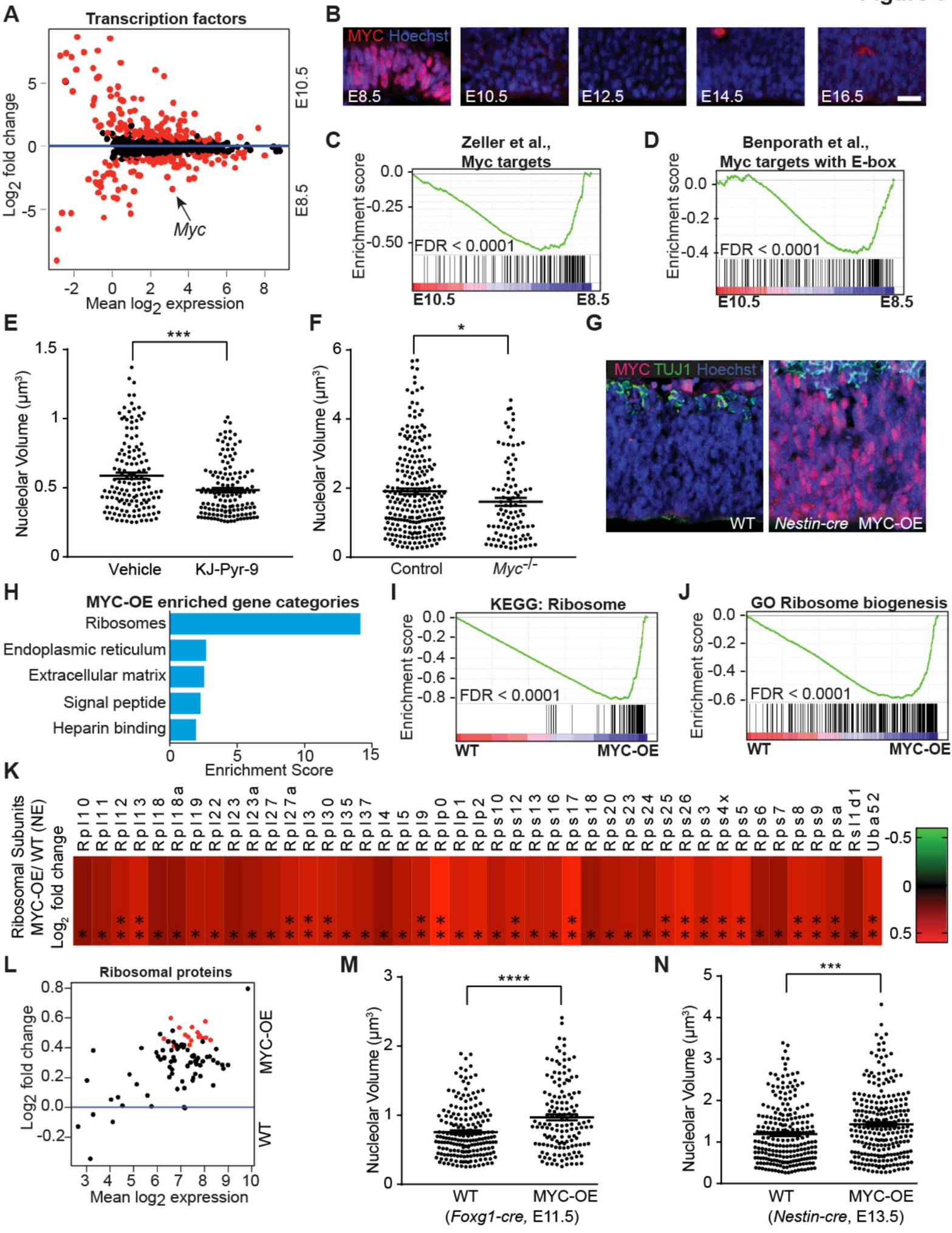
A
Transcription factors
Log2 fold change
Mean log2 expression
E10.5
E8.5
Myc
B
MYC Hoechst
E8.5
E10.5
E12.5
E14.5
E16.5
C
Zeller et al.,
Myc targets
Enrichment score
FDR < 0.0001
E10.5
E8.5
D
Benporath et al.,
Myc targets with E-box
Enrichment score
FDR < 0.0001
E10.5
E8.5
E
Nucleolar Volume (µm3)
***
Vehicle
KJ-Pyr-9
F
Nucleolar Volume (µm3)
*
Control
Myc-/-
G
MYC TUJ1 Hoechst
WT
Nestin-cre MYC-OE
H
MYC-OE enriched gene categories
Ribosomes
Endoplasmic reticulum
Extracellular matrix
Signal peptide
Heparin binding
Enrichment Score
I
KEGG: Ribosome
Enrichment score
FDR < 0.0001
WT
MYC-OE
J
GO Ribosome biogenesis
Enrichment score
FDR < 0.0001
WT
MYC-OE
K
Ribosomal Subunits
MYC-OE/ WT (NE)
Log2 fold change
Rpl10 Rpl11 Rpl12 Rpl13 Rpl18 Rpl18a Rpl19 Rpl22 Rpl23 Rpl23a Rpl27 Rpl27a Rpl3 Rpl30 Rpl35 Rpl37 Rpl4 Rpl5 Rpl9 Rplp0 Rplp1 Rplp2 Rps10 Rps12 Rps13 Rps16 Rps17 Rps18 Rps20 Rps23 Rps24 Rps25 Rps26 Rps3 Rps4x Rps5 Rps6 Rps7 Rps8 Rps9 Rpsa Rsl1d1 Uba52
L
Ribosomal proteins
Log2 fold change
Mean log2 expression
MYC-OE
WT
M
Nucleolar Volume (µm3)
****
WT
MYC-OE
(Foxg1-cre, E11.5)
N
Nucleolar Volume (µm3)
***
WT
MYC-OE
(Nestin-cre, E13.5)

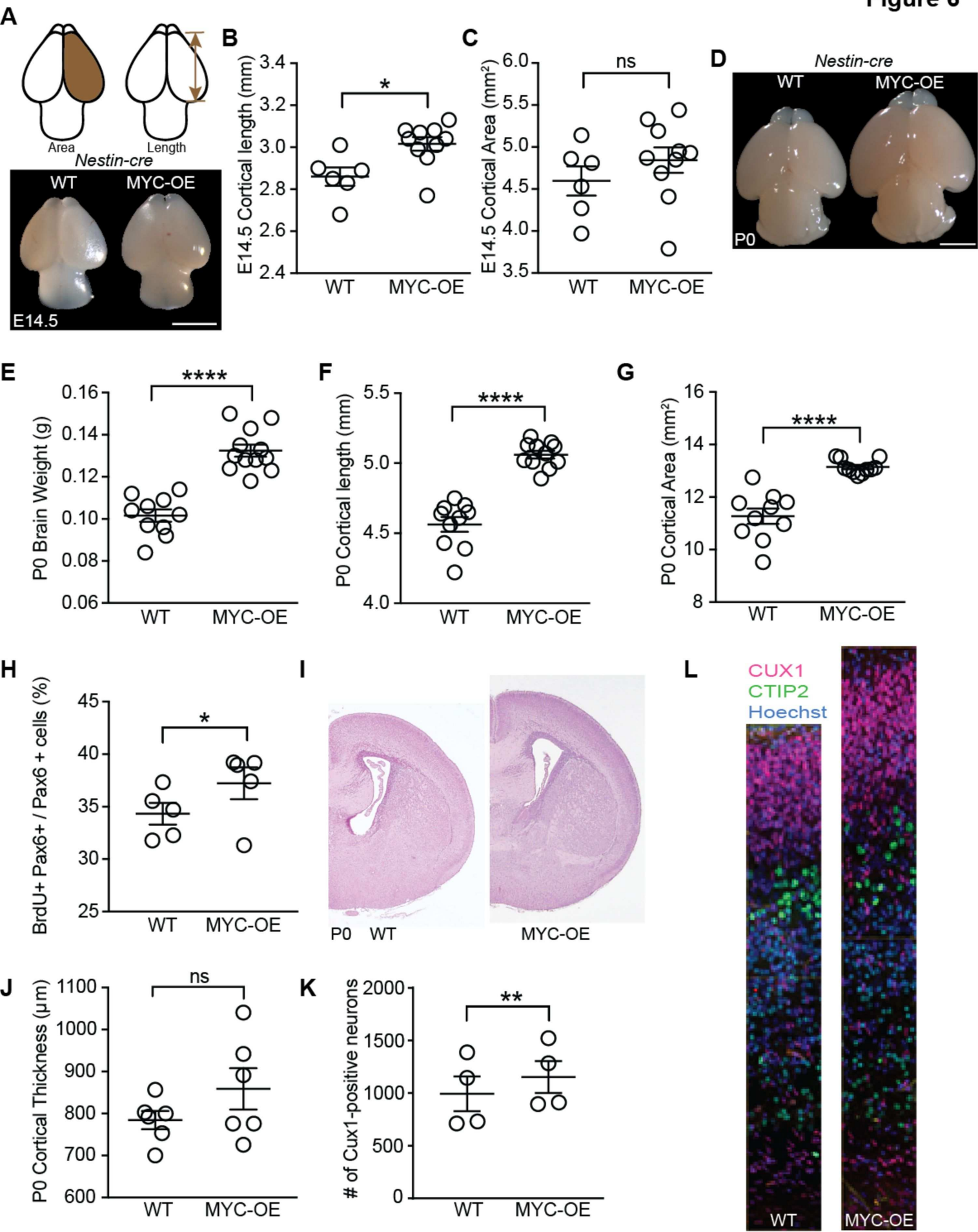
A
Area
Length
Nestin-cre
WT
MYC-OE
E14.5
B
E14.5 Cortical length (mm)
3.4
3.2
3.0
2.8
2.6
2.4
*
WT
MYC-OE
C
E14.5 Cortical Area (mm²)
6.0
5.5
5.0
4.5
4.0
3.5
ns
WT
MYC-OE
D
Nestin-cre
WT
MYC-OE
P0
E
P0 Brain Weight (g)
0.16
0.14
0.12
0.10
0.08
0.06
****
WT
MYC-OE
F
P0 Cortical length (mm)
5.5
5.0
4.5
4.0
****
WT
MYC-OE
G
P0 Cortical Area (mm²)
16
14
12
10
8
****
WT
MYC-OE
H
BrdU+ Pax6+ / Pax6 + cells (%)
45
40
35
30
25
*
WT
MYC-OE
I
P0
WT
MYC-OE
L
CUX1
CTIP2
Hoechst
WT
MYC-OE
J
P0 Cortical Thickness (µm)
1100
1000
900
800
700
600
ns
WT
MYC-OE
K
# of Cux1-positive neurons
2000
1500
1000
500
0
**
WT
MYC-OE

Figure 1-figure supplement 1

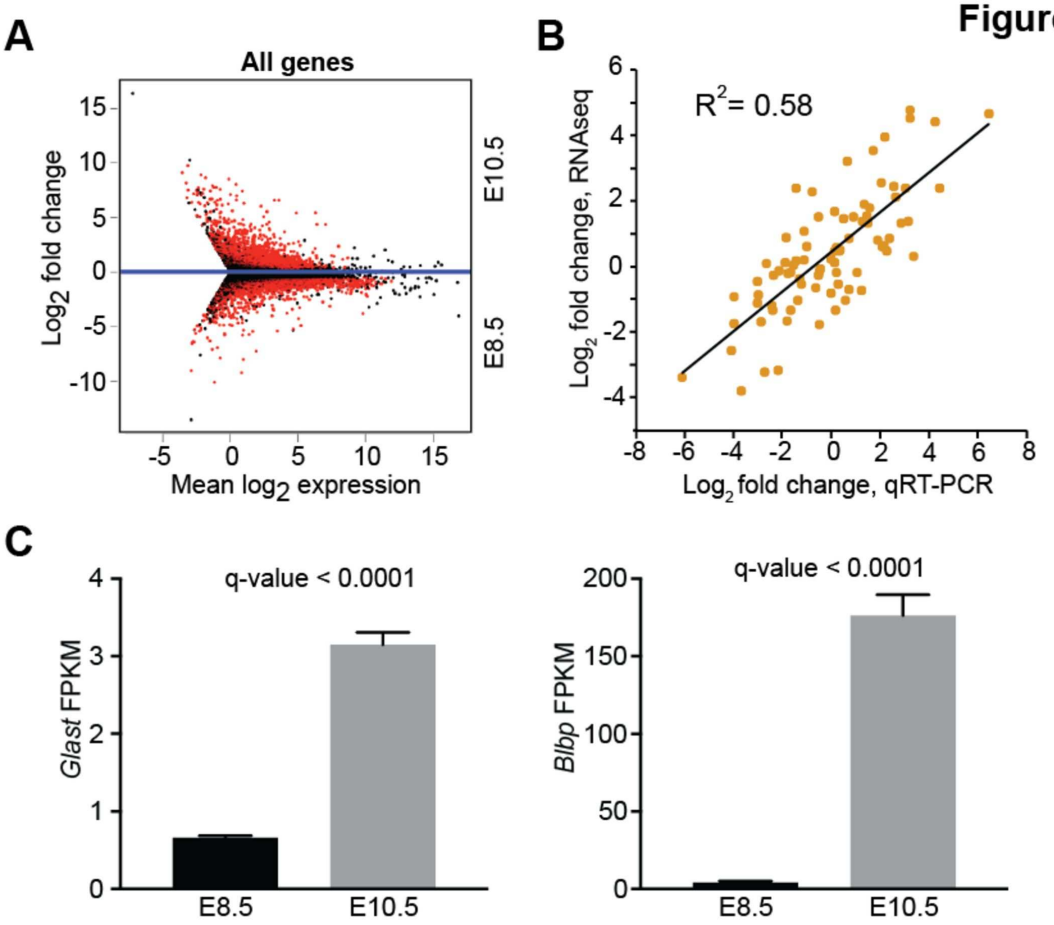

Figure 5-figure supplement 1

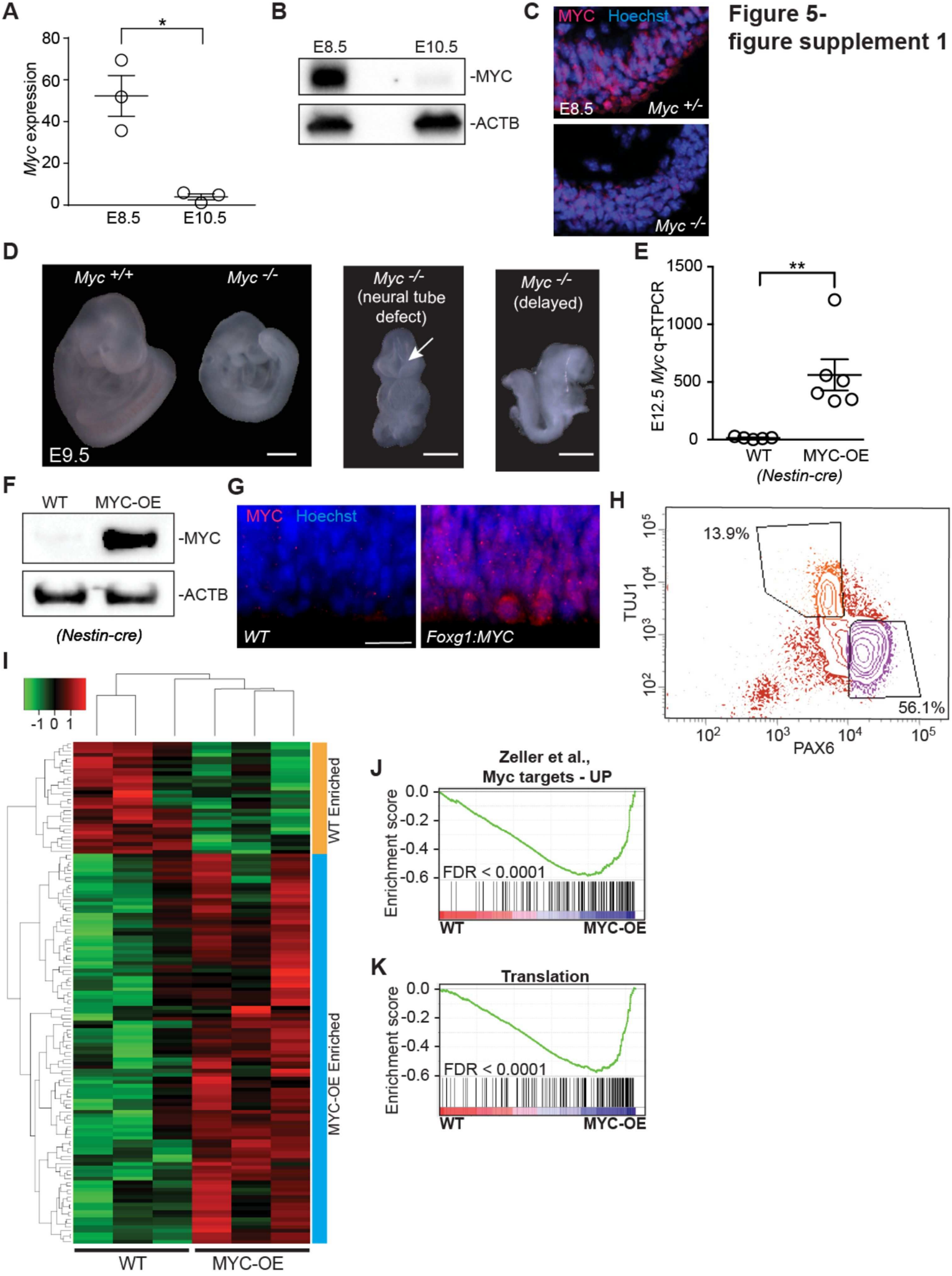

Figure 6-figure supplement 1